Thermodynamic Modeling of the Nickel-Lead-Tin System

G. GHOSH

A set of self-consistent thermodynamic model parameters is presented to describe the phase equilibria of nickel-lead (Ni-Pb) and nickel-tin (Ni-Sn) systems. Sublattice descriptions are used for thermodynamic modeling of the η-Ni_3Sn, λ-Ni_3Sn, η-Ni_3Sn_2, λ-Ni_3Sn_2, and Ni_3Sn_4 phases. A three-sublattice and a four-sublattice model are used to describe the molar Gibbs energies of η-Ni_3Sn_2 and λ-Ni_3Sn_2, respectively, and also to describe the second-order phase transition from η-Ni_3Sn_2 to λ-Ni_3Sn_2. In the majority of the cases, the agreement between the experimental data and the calculated values is very good. Since the experimental Ni-Pb-Sn ternary-phase diagrams are not known, several isothermal sections are calculated based on thermodynamic principles. They are of practical importance as related to microelectronics soldering applications.

I. INTRODUCTION

NICKEL-based metallization schemes, ranging from pure Ni to Cu-Ni, Ni-Pd, Ni-P, and Ni-V alloys, are either used or currently being developed for microelectronics packaging.[1,2] Even though Cu is the most commonly used solderable surface finish in printed circuit boards, Ni or a suitable Ni-based alloy is considered to be an excellent candidate for preventing excessive intermetallic formation. It is well known that the solders containing Sn react with Ni to form intermetallic(s) at the solder/metallization interface both during processing (or device fabrication) and in service. However, the rate of interfacial reaction is a strong function of processing and service temperatures and metallization and solder compositions. Often the interfacial reaction is exploited/controlled to obtain optimum properties of the joints. In the case of electronic packaging, it is very important to understand and control the interfacial microstructure formed due to the reaction between Ni and Pb-Sn or Pb-free solders.

Various phenomena governed by thermodynamic forces, such as interfacial reaction leading to the formation of new phase(s), wetting, and dewetting are of fundamental and practical interest to improve the reliability of microelectronic packaging. The strength and interfacial properties of the solder joints are determined by the interfacial microstructure. The evolution of the interfacial microstructure in solder joints is governed by the diffusion path during processing and in service. Even though the semiconductor industry uses a wide variety of complex metallization schemes, a thermodynamic description of the Ni-Pb-Sn system is needed to understand the interfacial microstructure of the real solder joints, since, in many cases, the metallization scheme contains Ni. Furthermore, the design of new metallization scheme(s) to control the interfacial microstructure and to improve the quality of solder joints is the cornerstone of advanced electronic packaging technology.

The Pb-Sn phase diagram is well studied, and, due to its simplicity, the thermodynamic description of the system exists in the literature.[3,4] The experimental phase-diagram data of Ni-Pb and Ni-Sn systems have been assessed by Nash[5] and Nash and Nash,[6] respectively. However, a comprehensive thermodynamic modeling of these two systems is still lacking. The objectives of this study are twofold: (1) to derive a set of self-consistent thermodynamic parameters to describe the phase equilibria in the Ni-Pb and Ni-Sn systems and (2) to calculate the Ni-Pb-Sn isothermal sections. Since the experimental Ni-Pb-Sn ternary-phase diagrams are not known, a convenient way to establish the phase relations is by calculations based on thermodynamic principles. Besides knowing the solubility of Ni in liquid Pb-Sn solders, isothermal sections are extremely helpful in interpreting the diffusion path (or the interfacial microstructure) during the interfacial reaction between Pb-Sn solders and the Ni substrate.

II. LITERATURE DATA

A. *Ni-Pb System*

The liquidus data have been reported by several investigators.[7–15] Portevin[9] and Voss[10] investigated the liquidus boundary of both Ni- and Pb-rich alloys. After applying an appropriate correction for temperature,[5] these two sets of data agree fairly well. Subsequent investigations[11–15] of the liquidus temperatures of Pb-rich alloys also agree very well with those reported by Portevin and Voss. The Ni-rich side is characterized by a monotectic reaction. Due to the presence of a liquid miscibility gap and a few liquidus data above 1423 K, the composition of the monotectic $liquid_{II}$ is somewhat uncertain.[5] The liquidus data of Portevin, Voss, and Miller and Elliot[13] give the monotectic temperature at 1613 ± 5 K.[5] Only Miller and Elliot established the presence of a liquid miscibility gap with a critical temperature around 1823 K. Their data suggest that the miscibility gap is asymmetric and skewed to the Ni-rich side. The Pb-rich side is characterized by a eutectic reaction.[5,9–11] The eutectic temperature was assessed to be 597 K.[5] The eutectic composition was reported to be 0.38 at. pct Ni[11] 0.46 at. pct Ni,[14] and 0.68 at. pct Ni.[5]

The solid solubility of Pb in (Ni) is not well established. Tammann and Bandel[16] noted that an alloy containing 0.57 at. pct Pb was single phase. Based on the duration of thermal arrests at the monotectic and eutectic temperatures, Voss[10]

G. GHOSH, Research Assistant Professor, is with the Department of Materials Science and Engineering, Robert R. McCormick School of Engineering and Applied Science, Northwestern University, Evanston, IL 60208-3108.

Manuscript submitted October 16, 1998.

concluded that the solubility of Pb in (Ni) was about 1.2 at. pct. Based on a thermodynamic analysis, Pomianek[17] suggested that the maximum solubility of Pb in (Ni) is about 0.9 at. pct.

The solid solubility of Ni in (Pb) was determined by magnetic[18] and resistivity[19] methods. Tammann and Oelsen[18] reported a maximum solid solubility of 0.68 at. pct, which is higher than the reported eutectic compositions; thus, it has been a subject of doubt.[20,21] Nozato *et al.*[19] found the solid solubility of Ni in (Pb) to be about an order of magnitude lower than that reported by Tammann and Oelsen.

There is no report of the existence of any equilibrium intermediate phase. Due to the liquid miscibility gap, rapid quenching from the liquid is difficult. Ricci-Bitti *et al.*[22] synthesized a metastable NiPb phase having an NiAs-type structure. The most likely origin of this phase has been discussed by Giessen.[23]

Cavanaugh and Elliot[7] carried out electromotive force (emf) measurements and determined the activities of Ni in the composition range from 1.36 to 11.1 at. pct Pb and in the temperature range from 973 to 1365 K. Their results indicate a large positive deviation from ideality. Pomianek[17] measured the activities of Pb in Ni-rich liquid alloys by the equilibrium vacuum saturation method. Their results also indicate a large positive deviation from ideality. Thermodynamic analysis of the phase diagram by Alden *et al.*,[8] Freedman and Nowick,[24] and Predel and Sandig[25] suggests a positive partial and molar enthalpy of mixing and also a positive excess entrophy of mixing.

B. *Ni-Sn System*

The phase equilibria were determined by a number of investigators using thermal analysis,[26–34] metallography,[28–30,33–35] chemical method,[36–40] and X-ray diffraction[33,34,41–47] techniques. Panteleimonov *et al.*[48] determined the phase relationships in alloys containing 20 to 30 at. pct Sn by means of differential thermal analysis, X-ray diffraction, and metallography techniques. The heating/cooling rate employed in the thermal analysis technique varied from 2 to 30 K/min,[31] 2 to 4 K/min,[33] and 1 to 2 K/min.[34] Thus, the results of Heumann[34] are believed to be more accurate. However, despite a difference in cooling rate by a factor of 2, the phase-boundary data of Mikulus *et al.*[33] and Heumann do not show a systematic variation over the whole composition range. Both Voss[30] and Mikulus *et al.* proposed the presence of two miscibility gaps, which was subsequently refuted by Heumann and Nial.[49] Furthermore, the phase diagram proposed by Mikulus *et al.* was inconsistent with the phase rule.[6]

Earlier investigations established the presence of three intermediate phases: Ni_3Sn,[27–30,35–40] Ni_3Sn_2,[28,29,30,36–40] and NiSn.[28,29,36–41] Furthermore, Voss[30] claimed the existence of Ni_4Sn. The presence of Ni_4Sn was also assumed by Mikulus *et al.*,[33] but refuted by Heumann[34] Also, the Ni_4Sn phase was replaced by a phase richer in Sn and Ni_3Sn_4.[33,34,44,45,49] Bhargava and Schubert[50] proposed that NiSn is stable below 873 K. It is very likely that NiSn is the result of a coring effect due to the peritectic reaction. The existence of only three intermediate phases (Ni_3Sn, Ni_3Sn_2, and Ni_3Sn_4) was further corroborated by Michel,[51] and these three phases are accepted for thermodynamic modeling.

Earlier work indicated that Ni_3Sn forms by a peritectic reaction,[28,29,30,33] but Heumann[34] showed that Ni_3Sn melts congruently. There are two forms of Ni_3Sn: the high-temperature form (η-Ni_3Sn) is stable between 1123 and 1147 K, and the low-temperature form (λ-Ni_3Sn) is stable below 1250 K. It has been argued that the transformation of η-Ni_3Sn to λ-Ni_3Sn is of the order-disorder type.[34,49,52]

Ni_3Sn_2 also melts congruently[34] around 1540 K. There are two forms of Ni_3Sn_2: the high-temperature form (η-Ni_3Sn_2) is stable between 873 and 1540 K, and the low-temperature form (λ-Ni_3Sn_2) is stable below 873 K.

Ni_3Sn_4 was first reported by Mikulus *et al.*,[33] and it forms by a peritectic reaction. In the vicinity of the Ni_3Sn_4 composition, Lihl and Kirnbauer [46,47] reported the existence of two intermediate "δ" phases having 51.8 $\pm$ 0.25 at. pct Sn and a structure identical to that of Ni_3Sn_4, and a "δ_1" phase having 54.8 at. pct Sn. A similar claim, though unsubstantiated, was also made by Fetz and Jette.[42,43] However, these results were inconclusive due to the lack of any thermal effects associated with the formation of the "δ_1" phase.[6]

The Ni-Sn system is further characterized by the presence of three eutectic reactions, L $\leftrightarrow$ (Ni) + η-Ni_3Sn,[33,34] L $\leftrightarrow$ η-Ni_3Sn + η-Ni_3Sn_2,[34] L $\leftrightarrow$ Ni_3Sn_4 + (Sn);[26,27,31] a peritectic reaction L + η-Ni_3Sn_2 $\leftrightarrow$ Ni_3Sn_4;[29,30,33,34] and two eutectoid reactions, η-Ni_3Sn $\leftrightarrow$ (Ni) + λ-Ni_3Sn[48] and η-Ni_3Sn $\leftrightarrow$ λ-Ni_3Sn + η-Ni_3Sn_2.[48]

The solid solubility of Sn in (Ni), between 773 and 1373 K, was determined by the lattice parameter method.[32,33] and also by X-ray diffraction and magnetometry[53] In general, there is a fairly good agreement between these data, except at low temperatures, where the data of Djega–Mariadassou[53] show a higher solid solubility. The solid solubility of Ni in (Sn) is not very well established. The only quantitative data of Hanson *et al.*[31] indicate that the solid solubility of Ni in (Sn) is less than 0.005 at. pct.

Eremenko *et al.*[54,55] determined the activity of Sn in liquid alloys at 1573 K, in the composition range from 12 to 82 at. pct Sn, by the emf method. Their data show a negative deviation and a positive deviation from ideality in the Ni-rich and Sn-rich alloys, respectively. The integral molar enthalpy of mixing (ΔH_m^{liq}) of liquid alloys was determined at 1773,[56] 1850,[57] 1580, [58] 1775,[59] 1702,[59] and 1660 K[59] by the calorimetric method. These results show that ΔH_m^{liq} is strongly negative, passes through a minimum around 40 at. pct Sn, and is temperature dependent. The heat of solution of Ni in liquid Sn at infinite dilution ($\Delta H_{Ni}^{liq,\infty}$) has been measured in the temperature range from 523 to 1100 K.[60–75] Compilation of $\Delta H_{Ni}^{liq,\infty}$ data suggests a scatter of 5 to 10 kJ/mole at any given temperature. Despite the scatter, the experimental data also suggest that $\Delta H_{Ni}^{liq,\infty}$ becomes more positive with increasing temperature. The partial molar heat of solution of Ni (ΔH_{Ni}^{liq}) in liquid alloys containing up to 14 at. pct Ni was measured at 1023[70] and 1095 K.[75] Once again, substantial scatter was noted in these measurements.

The heat of formation (ΔH_f) of the λ-Ni_3Sn, λ-Ni_3Sn_2, and Ni_3Sn_4 phases was reported at 273[55] and 298.15 K.[76,77] The heat of formation of the λ-Ni_3Sn_2 phase, reported by Predel and Ruge,[76] was about 8 kJ/mole more negative than a more recent measurement by Predel and Vogelbein.[77] The ΔH_f values of Koerber and Oelsen[56] and Predel and

Vogelbein agree very well. The ΔH_f values of the η-Ni_3Sn_2 and Ni_3Sn_4 phases were also measured at 1023 K.[70]

C. *Pb-Sn System*

All experimental data of this binary system have been compiled by Karakaya and Thompson.[3] A thermodynamic assessment of the system has been reported by Ngai and Chang.[4]

III. THERMODYNAMIC MODELING

A. *Pure Elements*

The pure solid elements at 298.15 K, in their stable forms, were chosen as the reference state of the system. The Scientific Group Thermodata Europe phase stabilities, for stable and metastable states of pure elements, published by Dinsdale,[78] are used. The lattice stability equations are given in the form $^{\circ}G_i(T) - H_i^{\mathrm{SER}}(298.15)$, where the stability of the phase is described relative to the stable-element reference at 298.15 K. The temperature dependence of the lattice stabilities are expressed as

$$^{\circ}G_i(T) - H_i^{\mathrm{SER}}(298.15) = A + BT + CT\ln T + DT^2 + ET^{-1} + FT^3 + IT^7 + JT^{-9} \quad [1]$$

where $H_i^{\mathrm{SER}}(298.15)$ is the enthalpy of the pure element (i) at the standard reference temperature.

B. *Solution Phases*

The liquid, fcc, and bct phases are considered as substitutional solutions, allowing complete mixing of Ni, Pb, and Sn on the same sublattice. The molar Gibbs energy of a solution phase (ϕ) can be expressed as

$$G_m^{\phi} - H^{\mathrm{SER}} = {}^{\mathrm{ref}}G + {}^{id}G^{\phi} + {}^{xs}G^{\phi} + {}^{\mathrm{mag}}G^{\phi} \quad [2a]$$

$${}^{\mathrm{ref}}G = \sum_{\mathrm{i}}[^{\circ}G_{\mathrm{i}}^{\mathrm{ref}}(T) - H_{\mathrm{i}}^{\mathrm{SER}}(298.15)]\cdot x_{\mathrm{i}} \quad [2b]$$

$${}^{id}G^{\phi} = RT[\sum_{\mathrm{i}} x_i \ln(x_{\mathrm{i}})] \quad [2c]$$

$${}^{xs}G^{\phi} = \sum_{\mathrm{i}\neq\mathrm{j}} x_{\mathrm{i}}x_{\mathrm{j}}[L^0 + (x_{\mathrm{i}} - x_{\mathrm{j}})L^1 + (x_{\mathrm{i}} - x_{\mathrm{j}})^2L^2 + \ldots] \quad [2d]$$

where i and j = Ni, Pb, and Sn; ${}^{\mathrm{ref}}G$ is the Gibbs energy of the reference state; ${}^{id}G^{\phi}$ is the ideal Gibbs energy of mixing; ${}^{xs}G^{\phi}$ is the excess Gibbs energy of mixing, which is expressed by a Redlich–Kister polynomial;[79] and ${}^{\mathrm{mag}}G^{\phi}$ is the magnetic contribution to the Gibbs energy. The interaction parameters L^k may be temperature dependent.

The magnetic contribution to the Gibbs energy of the fcc phase (Ni) is given by[80]

$${}^{\mathrm{mag}}G^{\mathrm{fcc}} = RT\ln(\beta + 1)f(\tau) \quad [3]$$

where $\tau = T/T_{\mathrm{C}}$, T_{C} is the Curie temperature, and β is the average magnetic moment in Bohr magneton. The function $f(\tau)$ for the fcc phase is given by[80]

$$f(\tau) = 1 - 0.24089\,\tau^{-1} - 0.17449\,\tau^{3} - 0.007755\,\tau^{9} - 0.001745\,\tau^{15};\ \text{for } \tau \le 1 \quad [4a]$$

$$f(\tau) = -0.04269\,\tau^{-5} - 0.0013552\,\tau^{-15}\ 0.0002846\,\tau^{-25};\ \text{for } \tau > 1 \quad [4b]$$

The composition dependence of T_{C} and β on fcc Ni-Sn alloys is described by

$$T_{\mathrm{C}}^{\mathrm{fcc}} = x_{\mathrm{Ni}}\,T_{\mathrm{C;Ni}} + x_{\mathrm{Ni}}x_{\mathrm{Sn}}[T^0_{\mathrm{C;Ni,Sn}} + (x_{\mathrm{Ni}} - x_{\mathrm{Sn}})\,T^1_{\mathrm{C;Ni,Sn}}] \quad [5]$$

$$\beta^{\mathrm{fcc-}} = x_{\mathrm{Ni}}\beta_{\mathrm{Ni}} + x_{\mathrm{Ni}}x_{\mathrm{Sn}}[\beta^0_{\mathrm{Ni,Sn}} + (x_{\mathrm{Ni}} - x_{\mathrm{Sn}})\,\beta^1_{\mathrm{Ni,Sn}}] \quad [6]$$

where $T_{\mathrm{C;Ni}}$ and β_{Ni} are the curie temperature and Bohr magneton of pure Ni, respectively. These values are adopted from Reference 81. The interaction parameters, such as $T^0_{\mathrm{C;Ni,Sn}}$, $T^1_{\mathrm{C;Ni,Sn}}$, *etc.*, are derived by optimizing the experimental data of Ni-Sn alloys.[53,82,83]

C. *η-Ni_3Sn and λ-Ni_3Sn Phases*

According to Schubert *et al.*,[84] η-Ni_3Sn has a cubic structure and it is isotypic with Fe_3Al (space group: $Fm\bar{3}m$), even though other structures have been reported in the literature.[48,85] In our thermodynamic modeling, the cubic structure is accepted. On the other hand, the structure of λ-Ni_3Sn is unambiguous. It has a hexagonal structure[34,47–49,51,52,86–88] and it is isotypic with Mg_3Cd (space group: $P6_3/mmc$). Experimental data show that η-Ni_3Sn and λ-Ni_3Sn have a homogeneity range on both sides of ideal stoichiometry. For example, according to Panteleimonov *et al.*,[48] the homogeneity ranges of η-Ni_3Sn and λ-Ni_3Sn are from 23 to 27.4 at. pct Sn and from 23.25 to 26.1 at. pct Sn, respectively. Accordingly, these two phases were modeled as (Ni, Sn)$_{0.75}$(Ni,Sn)$_{0.25}$. As an example, the molar Gibbs energy of η-Ni_3Sn is given by

$$\begin{aligned} ^{\circ}G_m^{\eta-\mathrm{Ni_3Sn}} = {} & Y^{\mathrm{I}}_{\mathrm{Ni}}Y^{\mathrm{II}}_{\mathrm{Ni}}\,^{\circ}G^{\eta-\mathrm{Ni_3Sn}}_{\mathrm{Ni:Ni}} + Y^{\mathrm{I}}_{\mathrm{Ni}}Y^{\mathrm{II}}_{\mathrm{Sn}}\,^{\circ}G^{\eta-\mathrm{Ni_3Sn}}_{\mathrm{Ni:Sn}} \\ & + Y^{\mathrm{I}}_{\mathrm{Sn}}Y^{\mathrm{II}}_{\mathrm{Ni}}\,^{\circ}G^{\eta-\mathrm{Ni_3Sn}}_{\mathrm{Sn:Ni}} + Y^{\mathrm{I}}_{\mathrm{Sn}}Y^{\mathrm{II}}_{\mathrm{Sn}}\,^{\circ}G^{\eta-\mathrm{Ni_3Sn}}_{\mathrm{Sn:Sn}} \\ & + 0.75\,\mathrm{R}T(Y^{\mathrm{I}}_{\mathrm{Ni}}\ln Y^{\mathrm{I}}_{\mathrm{Ni}} + Y^{\mathrm{I}}_{\mathrm{Sn}}\ln Y^{\mathrm{I}}_{\mathrm{Sn}}) \\ & + 0.25\,\mathrm{R}T(Y^{\mathrm{II}}_{\mathrm{Ni}}\ln Y^{\mathrm{II}}_{\mathrm{Ni}} + Y^{\mathrm{II}}_{\mathrm{Sn}}\ln Y^{\mathrm{II}}_{\mathrm{Sn}}) \\ & + Y^{\mathrm{I}}_{\mathrm{Ni}}Y^{\mathrm{II}}_{\mathrm{Ni}}Y^{\mathrm{II}}_{\mathrm{Sn}}L^{0,\eta-\mathrm{Ni_3Sn}}_{\mathrm{Ni:Ni,Sn}} + Y^{\mathrm{I}}_{\mathrm{Sn}}Y^{\mathrm{II}}_{\mathrm{Ni}}Y^{\mathrm{II}}_{\mathrm{Sn}}L^{0,\eta-\mathrm{Ni_3Sn}}_{\mathrm{Sn:Ni,Sn}} \\ & + Y^{\mathrm{I}}_{\mathrm{Ni}}Y^{\mathrm{I}}_{\mathrm{Sn}}Y^{\mathrm{II}}_{\mathrm{Ni}}L^{0,\eta-\mathrm{Ni_3Sn}}_{\mathrm{Ni,Sn:Ni}} + Y^{\mathrm{I}}_{\mathrm{Ni}}Y^{\mathrm{I}}_{\mathrm{Sn}}Y^{\mathrm{II}}_{\mathrm{Sn}}L^{0,\eta-\mathrm{Ni_3Sn}}_{\mathrm{Ni,Sn:Sn}} \end{aligned} \quad [7]$$

where $Y^{\mathrm{I}}_{\mathrm{i}}$ and $Y^{\mathrm{II}}_{\mathrm{i}}$ are the site fractions of element (representing Ni and Sn) on sublattice I and II, respectively; R is the universal gas constant; and T is the temperature in Kelvin. By convention, a comma and a semicolon separate elements on different sublattices and on the same sublattice, respectively. The parameters $^{\circ}G^{\eta-\mathrm{Ni_3Sn}}_{\mathrm{Ni:Ni}}$ and $^{\circ}G^{\eta-\mathrm{Ni_3Sn}}_{\mathrm{Sn:Sn}}$ denote the lattice stabilities of Ni and Sn, respectively, in the bcc structure. In the case of the λ-Ni_3Sn phase, the parameters $^{\circ}G^{\lambda-\mathrm{Ni_3Sn}}_{\mathrm{Ni:Ni}}$ and $^{\circ}G^{\lambda-\mathrm{Ni_3Sn}}_{\mathrm{Sn:Sn}}$ would represent the lattice stabilities of Ni and Sn, respectively, in the hcp structure. The parameters $^{\circ}G^{\eta-\mathrm{Ni_3Sn}}_{\mathrm{Ni:Sn}}$ and $^{\circ}G^{\eta-\mathrm{Ni_3Sn}}_{\mathrm{Sn:Ni}}$ denote the Gibbs energy of formation of Ni_3Sn and Sn_3Ni, respectively. Like the model for substitutional solutions, the interaction parameters $L^{0,\eta-\mathrm{Ni_3Sn}}_{\mathrm{Ni:Ni,Sn}}$, $L^{0,\eta-\mathrm{Ni_3Sn}}_{\mathrm{Sn:Ni,Sn}}$, *etc.*, may also be temperature dependent. The molar Gibbs energy of λ-Ni_3Sn is also expressed by an equation analogous to that given in Eq. [7].

D. *η-Ni_3Sn_2 and λ-Ni_3Sn_2 Phases*

The structure of η-Ni_3Sn_2 is hexagonal,[33,41,46,47,49,51,89–93] and it is isotypic with NiAs (space group: $P6_3/mmc$), having

partially filled sites. In thermodynamic modeling of the Pd-Pb-Sn system, we proposed a generic three-sublattice model applicable to all phases having either a NiAs-or Ni_2In type of structure.[94] The model was successfully applied to the β-Pd_5Pb_3, γ-Pd_5Pb_3, and γ-Pd_2Sn phases. Consistent with the NiAs-type structure, η-Ni_3Sn_2 is also modeled with three sublattices with the sublattice description $(Ni)_1(Sn)_1(Ni,Va)_1$, where *Va* stands for vacancy. This model restricts the homogeneity range from 33.33 to 50 at. pct Sn. The experimental homogeneity range of η-Ni_3Sn_2 was reported to vary from 36 to 40.5 at. pct Sn at 1433 K[34] from 38.4 to 42.5 at. pct Sn at 873 K,[49] and from 38.6 to 42.5 at. pct Sn.[46,47] Then, the molar Gibbs energy of η-Ni_3Sn_2 is expressed as

$$\begin{aligned}{}^{\circ}G_m^{\eta-Ni_3Sn_2} = {} & Y_{Ni}^{III}\,{}^{\circ}G_{Ni:Sn:Ni}^{\eta-Ni_3Sn_2} + Y_{Va}^{III}\,{}^{\circ}G_{Ni:Sn:Va}^{\eta-Ni_3Sn_2} \\ & + RT(Y_{Ni}^{III}\ln Y_{Ni}^{III} + Y_{Va}^{III}\ln Y_{Va}^{III}) \\ & + Y_{Ni}^{III}Y_{Va}^{III}[L_{Ni:Sn:Ni,Va}^{0,\eta-Ni_3Sn_2} \\ & + (Y_{Ni}^{III} - Y_{Va}^{III})L_{Ni:Sn:Ni,Va}^{1,\eta-Ni_3Sn_2}]\end{aligned} \quad [8]$$

where Y_i^{III} is the site fraction of *i* (representing Ni and *Va*) in the third sublattice; ${}^{\circ}G_{Ni:Sn:Ni}^{\eta-Ni_3Sn_2}$ is the Gibbs energy of formation of η-Ni_3Sn_2 at Ni_2Sn, *i.e.*, when the third sublattice is completely occupied by Ni only; and ${}^{\circ}G_{Ni:Sn:Va}^{\eta-Ni_3Sn_2}$ is the Gibbs energy of formation of η-Ni_3Sn_2 at NiSn, *i.e.*, when the third sublattice is completely occupied by vacancies only. Besides the η-Ni_3Sn_2, β-Pd_5Pb_3, γ-Pd_5Pb_3, and γ-Pd_2Sn phases, the aforementioned three-sublattice model has also been applied to the Cu_6Sn_5 and AuSn phases.[95]

It has been reported that η-Ni_3Sn_2 undergoes superstructural ordering of the occupied and vacant sites within the metal sublattices to form λ-Ni_3Sn_2 at around 873 K[49,51,90,91,96,97] and it is believed to be second-order. However, Fjellvag and Kjekshus[92] have argued that the η-Ni_3Sn_2 to λ-Ni_3Sn_2 phase transition may be first-order. λ-Ni_3Sn_2 has an orthorhombic structure with space group *Pnma*. Since *Pnma* is a subgroup of $P6_3/mmc$ (the space group of η-Ni_3Sn_2), the possibility of a second-order transition seems to be favorable. The relationships between the lattice parameters of orthorhombic λ-Ni_3Sn_2 and hexagonal η-Ni_3Sn_2 are $\mathbf{a}_o \approx \sqrt{3}\mathbf{a}_h$, $\mathbf{b}_o \approx 2\mathbf{a}_h$, $\mathbf{c}_o \approx \mathbf{c}_h$, and $V_o \approx 4V_h$, where *o* and *h* represent orthorhombic and hexagonal, respectively. This means that, during the ordering process, the *c*-axis of the disordered hexagonal structure becomes the *c*-axis of the ordered orthorhombic structure, while the hexagonal *a*-axis becomes orthorhombic *b*-axis.

To model the η-Ni_3Sn_2 to λ-Ni_3Sn_2 second-order transition, we adopt the Bragg–Williams–Gorsky treatment of the composition-dependent, long-range ordering contribution between Ni and *Va* in a manner analogous to the model used to describe the A2 ↔ B2 second-order transition in Fe-Si,[98] Al-Fe,[99] and Cu-Zn[100] alloys. Thus, the sublattice description of λ-Ni_3Sn_2 is $(Ni)_1(Sn)_1(Ni,Va)_{0.5}(Ni,Va)_{0.5}$. Then, the molar Gibbs energy of λ-Ni_3Sn_2 is expressed as

$$\begin{aligned}{}^{\circ}G_m^{\lambda-Ni_3Sn_2} = {} & Y_{Ni}^{III}Y_{Ni}^{IV}\,{}^{\circ}G_{Ni:Sn:Ni:Ni}^{\lambda-Ni_3Sn_2} + Y_{Ni}^{III}Y_{Va}^{IV}\,{}^{\circ}G_{Ni:Sn:Ni:Va}^{\lambda-Ni_3Sn_2} \\ & + Y_{Va}^{III}Y_{Ni}^{IV}\,{}^{\circ}G_{Ni:Sn:Va:Ni}^{\lambda-Ni_3Sn_2} + Y_{Va}^{III}Y_{Va}^{I}\,{}^{\circ}G_{Ni:SnVa:Va}^{\lambda-Ni_3Sn_2} \\ & + 0.5\,RT(Y_{Ni}^{III}\ln Y_{Ni}^{III} + Y_{Va}^{III}\ln Y_{Va}^{III} \\ & + Y_{Ni}^{IV}\ln Y_{Ni}^{IV} + Y_{Va}^{IV}\ln Y_{Va}^{IV}) \\ & + Y_{Ni}^{III}Y_{Va}^{III}Y_{Ni}^{IV}[L_{Ni:Sn:Ni,\ Va:Ni}^{0,\lambda-Ni_3Sn_2} \\ & + (Y_{Ni}^{III} - Y_{Va}^{III})L_{Ni:Sn:Ni,Va:Ni}^{1,\lambda-Ni_3Sn_2}] \\ & + Y_{Ni}^{III}Y_{Va}^{III}Y_{Va}^{IV}[L_{Ni:Sn:Ni,Va:Va}^{0,\lambda-Ni_3Sn_2} \\ & + (Y_{Ni}^{III} - Y_{Va}^{III})L_{Ni:Sn:Ni,Va:Va}^{1,\lambda-Ni_3Sn_2}] \\ & + Y_{Ni}^{III}Y_{Ni}^{IV}Y_{Va}^{IV}[L_{Ni:Sn:Ni:Ni,Va}^{0,\lambda-Ni_3Sn_2} \\ & + (Y_{Ni}^{IV} - Y_{Va}^{IV})L_{Ni:Sn:Ni:Ni,Va}^{1,\lambda-Ni_3Sn_2}] \\ & + Y_{Va}^{III}Y_{Ni}^{IV}Y_{Va}^{IV}[L_{Ni:Sn:Va:Ni,Va}^{0,\lambda-Ni_3Sn_2} \\ & + (Y_{Ni}^{IV} - Y_{Va}^{IV})L_{Ni:SnVa:Ni,Va}^{1,\lambda-Ni_3Sn_2}]\end{aligned} \quad [9]$$

where Y_i^{III} and Y_i^{IV} are the site fractions of *i* (representing Ni and *Va*) in the third and fourth sublattice, respectively. It is possible to show that the Gibbs energy parameters of λ-Ni_3Sn_2 in Eq. [9] are related to those of η-Ni_3Sn_2 in Eq. [8] and an ordering energy contribution (ΔW), yielding the following relations:

$${}^{\circ}G_{Ni:Sn:Ni:Ni}^{\lambda-Ni_3Sn_2} = {}^{\circ}G_{Ni:Sn:Ni}^{\eta-Ni_3Sn_2} \quad [10]$$

$$\begin{aligned}{}^{\circ}G_{Ni:Sn:Ni:Va}^{\lambda-Ni_3Sn_2} = {}^{\circ}G_{Ni:Sn:Va:Ni}^{\lambda-Ni_3Sn_2} &= \Delta W + 0.5\,{}^{\circ}G_{Ni:Sn:Ni}^{\eta-Ni_3Sn_2} \\ & + 0.5\,{}^{\circ}G_{Ni:Sn:Va}^{\eta-Ni_3Sn_2} + 0.25\,L_{Ni:Sn:Ni,Va}^{0,\eta-Ni_3Sn_2}\end{aligned} \quad [11]$$

$${}^{\circ}G_{Ni:Sn:Va:Va}^{\lambda-Ni_3Sn_2} = {}^{\circ}G_{Ni:Sn:Va}^{\eta-Ni_3Sn_2} \quad [12]$$

$$\begin{aligned}L_{Ni:Sn:Ni,Va:Ni}^{0,\lambda-Ni_3Sn_2} &= L_{Ni:Sn:Ni:Ni,Va}^{0,\lambda-Ni_3Sn_2} \\ &= -\Delta W + 0.25\,L_{Ni:Sn:Ni,Va}^{0,\eta-Ni_3Sn_2} \\ &\quad + 0.375\,L_{Ni:Sn:Ni,Va}^{1,\eta-Ni_3Sn_2}\end{aligned} \quad [13]$$

$$\begin{aligned}L_{Ni:Sn:Ni,Va:Va}^{0,\lambda-Ni_3Sn_2} &= L_{Ni:Sn:Va:Ni,Va}^{0,\lambda-Ni_3Sn_2} \\ &= -\Delta W + 0.25\,L_{Ni:Sn:Ni,Va}^{0,\eta-Ni_3Sn_2} \\ &\quad - 0.375\,L_{Ni:Sn:Ni,Va}^{1,\eta-Ni_3Sn_2}\end{aligned} \quad [14]$$

$$\begin{aligned}L_{Ni:Sn:Ni,Va:Ni}^{1,\lambda-Ni_3Sn_2} &= L_{Ni:Sn:Ni,Va:Va}^{1,\lambda-Ni_3Sn_2} = L_{Ni:Sn:Ni:Ni,Va}^{1,\lambda-Ni_3Sn_2} = L_{Ni:Sn:Va:Ni,Va}^{1,\lambda-Ni_3Sn_2} \\ &= 0.125\ L_{Ni:Sn:Ni,Va}^{1,\eta-Ni_3Sn_2}\end{aligned} \quad [15]$$

Figure 1 is a plot of Y_{Ni}^{III} *vs* Y_{Ni}^{IV}, showing all possible combinations of Y_{Ni}^{III} and Y_{Ni}^{IV}, for different Sn contents, in λ-Ni_3Sn_2. The disordered state (η-Ni_3Sn_2) is given by the diagonal in Figure 1, where $Y_{Ni}^{III} = Y_{Ni}^{IV}$ and $Y_{Va}^{III} = Y_{Va}^{IV}$, and an off-diagonal point represents the ordered state (λ-Ni_3Sn_2). Above the critical temperature for ordering, the Gibbs energy of η-Ni_3Sn_2, given by Eq. [8], will be identical to that of λ-Ni_3Sn_2, given by Eqs. [10] through [15], and the energy minimum will lie along the diagonal. Below the critical temperature, λ-Ni_3Sn_2 will have a lower Gibbs energy than η-Ni_3Sn_2, and the energy minimum will lie along a nondiagonal locus in which the exact point will be determined by the temperature and the overall Sn content.

E. *Ni_3Sn_4 Phase*

This phase was first reported by Mikulus *et al.*[33] Ni_3Sn_4 has complex monoclinic structure (space group: $C2/m$), and it is isotypic with either Ni_3Sn_4, containing 14 atoms per unit cell,[101,102,103] or CoGe, containing 16 atoms per unit cell.[104] Experimental data show that the solid solubility of Ni_3Sn_4 extends toward the Ni side only[34,101,102] For example, the composition of Ni_3Sn_4 varies from 55.5 at. pct Sn at 1068 K to about 56.3 to 57.2 at. pct Sn at 773 K.[34] To

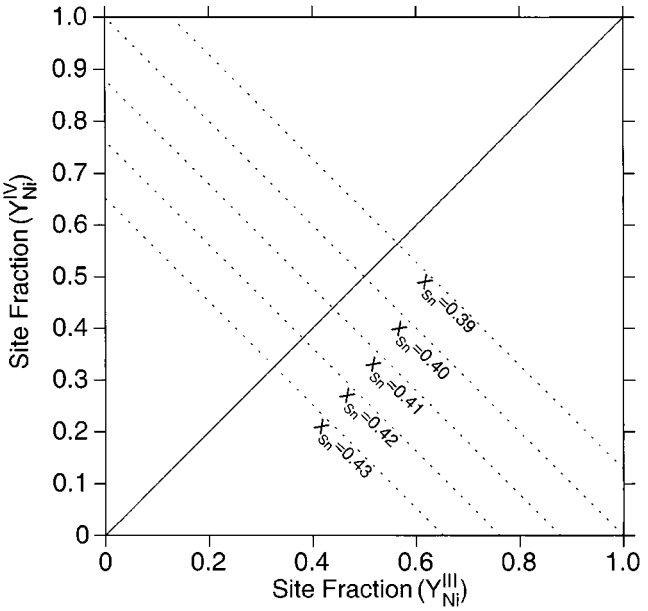

Fig. 1—The composition plane Y_{Ni}^{III} *vs* Y_{Ni}^{IV} corresponding to various mole fractions of Sn in the ordered λ-Ni_3Sn_2 phase. The diagonal ($Y_{Ni}^{III} = Y_{Ni}^{IV}$) represents the locus of composition of the disordered η-Ni_3Sn_2 phase.

account for the solid solubility, we adopt a simple two-sublattice model $(Ni)_{0.4286}(Ni,Sn)_{0.5714}$. The molar Gibbs energy is given by

$$^{\circ}G_m^{Ni_3Sn_4} = Y_{Ni}^{II}\,{}^{\circ}G_{Ni:Ni}^{Ni_3Sn_4} + Y_{Sn}^{II}\,{}^{\circ}G_{Ni:Sn}^{Ni_3Sn_4} + 0.5714\,RT(Y_{Ni}^{II}\ln Y_{Ni}^{II} + Y_{Sn}^{II}\ln Y_{Sn}^{II}) + Y_{Ni}^{II}Y_{Sn}^{II}[L_{Ni:Ni,Sn}^{0,Ni_3Sn_4} + (Y_{Ni}^{II} - Y_{Sn}^{II})L_{Ni:Ni,Sn}^{1,Ni_3Sn_4}] \quad [16]$$

where $^{\circ}G_{Ni:Ni}^{Ni_3Sn_4}$ is the lattice stability of Ni in the structure of Ni_3Sn_4, $^{\circ}G_{Ni:Sn}^{Ni_3Sn_4}$ is the Gibbs energy of formation of Ni_3Sn_4, and $L_{Ni:Ni,Sn}^{0,Ni_3Sn_4}$ and $L_{Ni:Ni,Sn}^{1,Ni_3Sn_4}$ are the sublattice interaction parameters.

IV. OPTIMIZATION OF LITERATURE DATA

Optimization of experimental data was carried out using the PARROT[105] module of the ThermoCalc software.[106] For the optimization of model parameters of the Ni-Pb system, the activity data,[7,17] the liquidus data,[7–15] and the invariant equilibria involving the liquid phase[5] were used. However, two experimental points of Voss[10] showed significant scatter, and they were not used for optimization.

At first, all experimental data were considered for the optimization of model parameters of the Ni-Sn system. However, incompatibilities between various sets of data were noticed during optimization. The final optimization was carried out using the activity data for the liquid phase,[54,55] the heat-of-mixing data for the liquid phase,[56,58] the heat of solution of Ni in liquid Sn,[61–75] the heat of formation of the intermediate phases,[56,77] and the phase-diagram data.[33,34,53] The model parameters $^{\circ}G_{Sn:Ni}^{\eta-Ni_3Sn}$ and $^{\circ}G_{Sn:Ni}^{\lambda-Ni_3Sn}$ represent the Gibbs energies when both sublattices are occupied by antistructure atoms only. Adopting the procedure of Bolcavage and Kattner,[107] these were estimated from the following constraints:

$$^{\circ}G_{Sn:Ni}^{\eta-Ni_3Sn} = {}^{\circ}G_{Ni:Ni}^{\eta-Ni_3Sn} + {}^{\circ}G_{Sn:Sn}^{\eta-Ni_3Sn} - {}^{\circ}G_{Ni:Sn}^{\eta-Ni_3Sn} \quad [17]$$

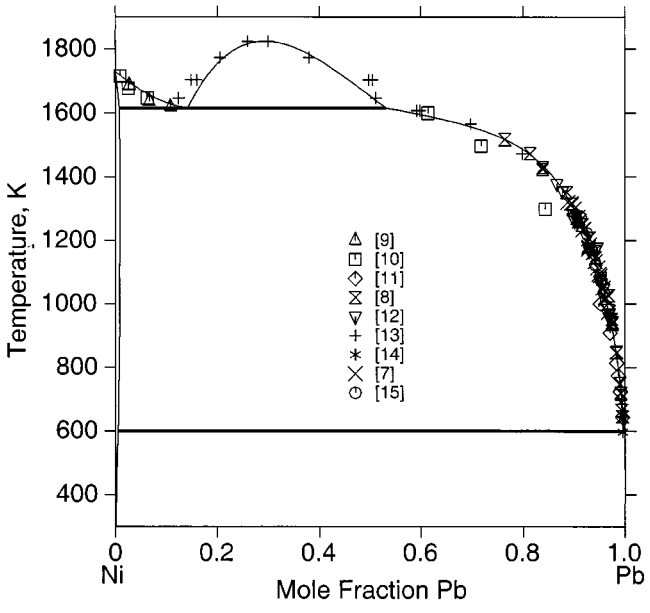

(*a*)

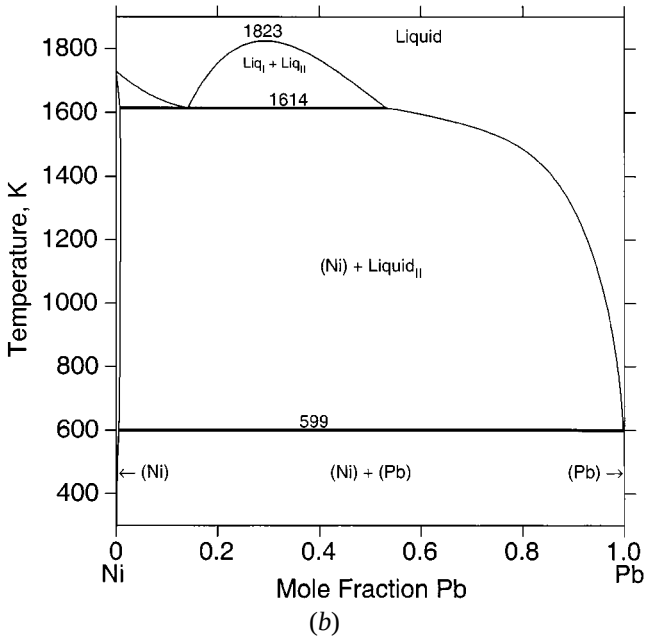

(*b*)

Fig. 2—The calculated Ni-Pb phase diagram (*a*) with experimetal points[7–15] and (*b*) without experimental points.

$$^{\circ}G_{Sn:Ni}^{\lambda-Ni_3Sn} = {}^{\circ}G_{Ni:Ni}^{\lambda-Ni_3Sn} + {}^{\circ}G_{Sn:Sn}^{\lambda-Ni_3Sn} - {}^{\circ}G_{Ni:Sn}^{\lambda-Ni_3Sn} \quad [18]$$

where $^{\circ}G_{i:i}^{\eta-Ni_3Sn}$ and $^{\circ}G_{i:i}^{\lambda-Ni_3Sn}$ are the molar Gibbs energies of element i(representing Ni and Sn) in its bcc and hcp structure, respectively.

All model parameters are listed in the Appendix.

V. RESULTS AND DISCUSSION

Figures 2(a) and (b) show the calculated Ni-Pb phase diagrams with and without experimental data, respectively. In general, the agreement between the calculated and experimental phase boundaries is very good. The experimental data clearly suggest an asymmetric liquid miscibility gap,

Table I. A Comparison of Calculated and Assessed Equilibria in the Ni-Pb System

Reaction	Temperature, K	Compositions* (in Mole Fraction of Pb)			Reference
$L_1 \leftrightarrow L_2 + (Ni)$	1613	0.1156	0.5700	0.0120	5
	1614	0.1412	0.5323	0.0077	this study
$L \leftrightarrow (Ni) + (Pb)$	597	0.9954	≈0.000	0.9983	5
	599.6	0.9971	0.0049	0.9989	this study
$L \leftrightarrow Liq_I + Liq_{II}$	1828		≈0.2900		5
	1824		0.2940		this study

*In the same sequence as the phases appear in the reaction.

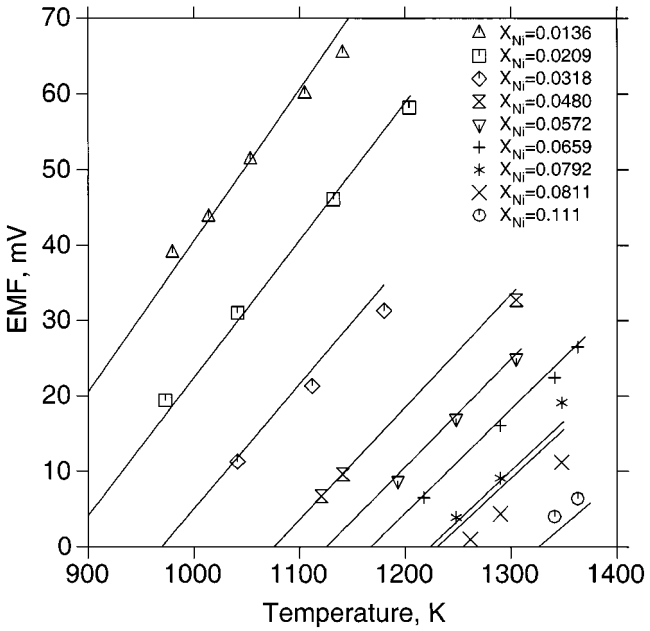

Fig. 3—Comparison of calculated emf (solid line) with the experimental data[7] in liquid Ni-Pb alloys as a function of temperature. The reference states are fcc-Ni and liquid-Pb.

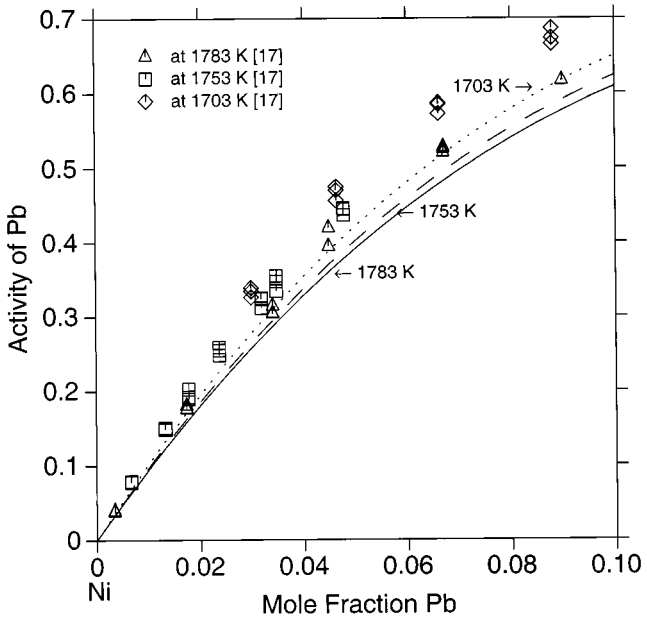

Fig. 4—Comparison of calculated activity of Pb in liquid Ni-Pb alloys with the experimental data.[17] The reference states are liquid-Ni and liquid-Pb at 1783 and 1753 K and fcc-Ni and liquid-Pb at 1703 K.

which is nicely reproduced in the calculated phase diagram. Both the critical temperature of the miscibility gap and the monotectic temperature are in excellent agreement with the assessed values of Nash.[5] A comparison of calculated and experimental invariant equilibria is listed in Table I. As mentioned by Nash, the composition of $liquid_{II}$ of the monotectic reaction is somewhat uncertain.

Figure 3 shows the temperature dependence of emf values in liquid Ni-Pb alloys at different Ni contents. Once again, the agreement between the calculated and experimental values[7] is very good. The calculated activities of Pb in liquid Ni-Pb alloys are compared to the experimental data[17] in Figure 4. The experimental values suggest a stronger positive deviation from ideality than those calculated from the optimized parameters. It is important to bear in mind that Pomianek[17] determined the activity coefficients by an isopiestic method, which is an equilibrium method. Despite its general advantage over Knudsen effusion or with the transportation method, a systematic error can be introduced through thermochemical data of the reference solution in the isopiestic method. Based on the optimized thermodynamic parameters presented in the Appendix, the maximum integral molar enthalpy of mixing of liquid is predicted to be 5.312 kJ/mole. This is in qualitative agreement with the values of 8.34 kJ/mole proposed by Nash[5] and 11.5 kJ/mole proposed by Predel and Sandig.[25] The calculated enthalpy of solution of Ni in liquid Pb at infinite dilution ($\Delta H_{Ni}^{liq,\infty}$) is found to 26.9 kJ/mol in the temperature range from 700 to 1000 K. Based on the thermodynamic analysis of the liquidus of the Pb corner, the previous estimates of $\Delta H_{Ni}^{liq,\infty}$ were 26.46[8] and 42.28 kJ/mol.[25]

It is to be noted that the liquid phase was modeled with nine adjustable parameters, while the solid phase was modeled using subregular interaction parameters. Although the available experimental thermodynamic data for the liquid phase could be fitted with fewer parameters, the use of nine parameters was dictated by the asymmetric miscibility gap and the overall shape of the liquidus. Due to the very good agreement between the calculated phase diagram and the experimental values in the entire composition range, and also between the calculated and experimental thermodynamic data of Pb-rich alloys,[7] we conclude that the thermodynamic properties of Ni-rich alloys deserve further investigation. Additionally, experimental thermodynamic data, such as enthalpy of mixing and activity data over the entire composition range, will aid in further refinement of the model parameters.

Figures 5(a) and (b) show the calculated Ni-Sn phase

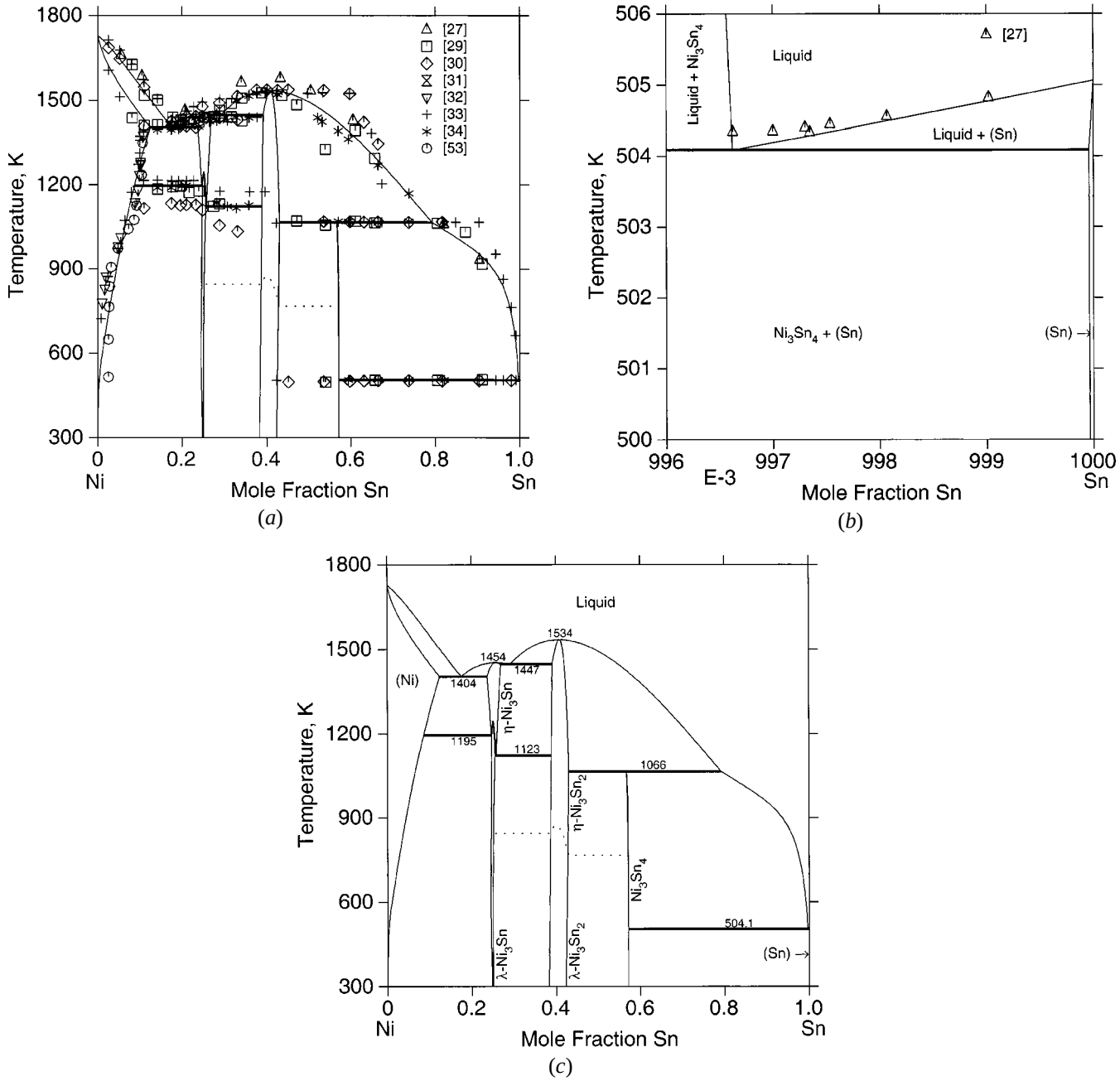

Fig. 5—The calculated Ni-Sn phase diagrams: (*a*) with experimetal points,[27,29–34,53] (*b*) an enlarged Sn-corner with experimental points,[27] and (*c*) without experimental points.

diagrams with experimental data. The presence of a eutectic in the Sn corner of the calculated diagram may be noted in Figure 5(b). Figure 5(c) shows the calculated Ni-Sn phase diagram without experimental data. The calculated and experimental equilibria of the Ni-Sn phase are compared in Table II. Despite significant scatter in the experimental data in a certain composition range, the overall agreement between the calculated phase boundaries and the experimental data in Figure 5(a) is considered to be good. A maximum solid solubility of 10.6 at. pct Sn[34] in (Ni) agrees satisfactorily with the calculated value of 12.2 at. pct Sn at the eutectic temperature. Also, the calculated solid solubility of 0.0037 at. pct Ni in (Sn) at 504 K is in good agreement with the experimental value of 0.005 at. pct.[31] Figures 6(a) and (b) show the composition dependence of the Curie temperature and magnetic moment of fcc Ni-Sn alloys, respectively. The T_c values reported by Djega-Mariadassou[53] are believed to be more accurate than others, as the alloys were heat treated in the single-phase field at 1343 K and quenched.

Figure 7 shows an excellent agreement between the calculated and experimental[55] activity of Sn in liquid Ni-Sn alloys. Figure 8 shows the calculated enthalpy of mixing of liquid Ni-Sn alloys (ΔH_m^{liq}) at 1580 and 1850 K. The calculated values agree very well with the experimental data of Esin *et al.*[57] and Luck *et al.*[59] In the composition range from 20 to 60 at. pct Sn, the data of Pool *et al.*[58] appears to be too negative. It is believed that the measurements of Luck *et al.* are more accurate than those of Pool *et al.*

Table II. A Comparison of Calculated and Experimental Equilibria in the Ni-Sn System

Reaction	Temperature, K	Compositions* (in Mole Fraction of Sn)			Reference
$L \leftrightarrow$ (Ni) + η-Ni_3Sn	1403	0.1909	—	0.2479	34
	1404	0.1759	0.1246	0.2369	this study
$L \leftrightarrow \eta$-Ni_3Sn + η-Ni_3Sn_2	1433	0.2725	0.2680	0.3570	34
	1447	0.2911	0.2689	0.3916	this study
L + η-$Ni_3Sn_2 \leftrightarrow Ni_3Sn_4$	1066	0.9038	0.4000	0.5714	33
	1067.5	0.8097	0.4197	0.5428	34
	1066	0.7925	0.4309	0.5673	this study
$L \leftrightarrow Ni_3Sn_4$ + (Sn)	504.2	0.9970	—	—	26
	505	0.9965	—	—	31
	504.1	0.9966	0.5714	0.9999	this study
η-$Ni_3Sn \leftrightarrow$ (Ni) + λ-Ni_3Sn	1193	0.2325	—	0.2380	48
	1195	0.2461	0.0867	0.2476	this study
η-$Ni_3Sn \leftrightarrow \lambda$-$Ni_3Sn$ + η-Ni_3Sn_2	1123	0.2725	0.2605	—	48
	1123	0.2576	0.2554	0.3887	this study
λ-$Ni_3Sn \leftrightarrow \eta$-$Ni_3Sn$	1223	—	0.2500	—	84
	1250	—	0.2500	—	48
	1246	—	0.2507	—	this study
$L \leftrightarrow \eta$-Ni_3Sn	1447	—	0.2500	—	34
	1454	—	0.2522	—	this study
$L \leftrightarrow \eta$-Ni_3Sn_2	1567	—	0.4000	—	34
	1534	—	0.4037	—	this study

*In the same sequence as the phases appear in the reaction.

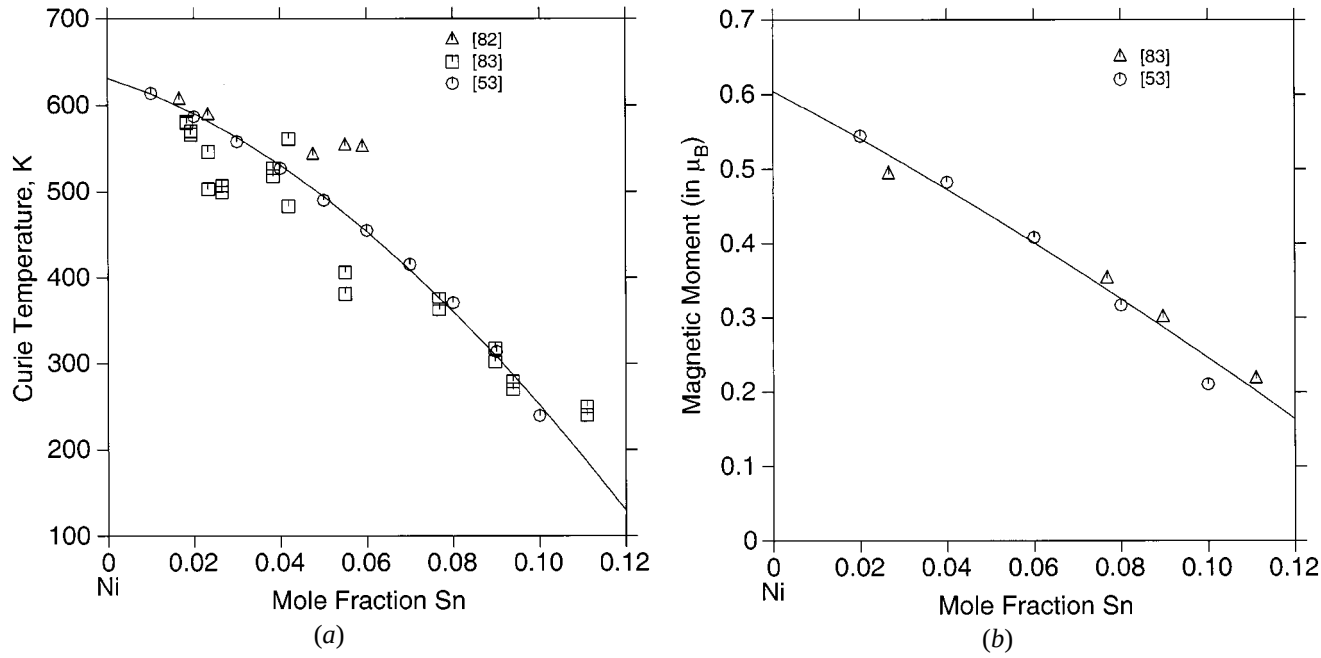

Fig. 6—The composition dependence of (*a*) the Curie temperature of fcc Ni-Sn alloys[53,82,83] and (*b*) the magnetic moment.[53,83]

The temperature dependence of the calculated enthalpy of solution of Ni in liquid Sn at infinite dilution ($\Delta H_{Ni}^{liq,\infty}$) is compared to the experimental values[60–75] in Figure 9, and the agreement is considered to be good. The experimental value of Leach and Bever[60] is far-less negative than others. Agrawal *et al.*[108] used a thermodynamic model to calculate the heat of mixing of liquid Ni-Sn alloys at 1773 K. They predicted $\Delta H_{Ni}^{liq,\infty}$ to be −41.25 kJ/mole at 1773 K. This value of $\Delta H_{Ni}^{liq,\infty}$ is far too negative compared to our calculated value of −24.83 kJ/mole and also compared to the value obtained by linear extrapolation of the experimental data. Figure 10 shows the partial molar enthalpy of Ni (ΔH_{Ni}^{liq}) in liquid Ni-Sn alloys at 1023[70] and 1095 K[75] as a function of Ni content. Due to substantial scatter in the data, the agreement is considered to be only satisfactory. However, both sets of data seem to suggest that ΔH_{Ni}^{liq} passes through a minimum at around 10 at. pct Ni. The calculated ΔH_{Ni}^{liq} curves also show this trend. Table III compares the optimized values of the heat of formation of Ni-Sn intermediate phases to the experimental values[56,70,76,77] and those predicted by de Boer *et al.*[109] The optimized ΔH_f values are in very good agreement with those reported by Predel

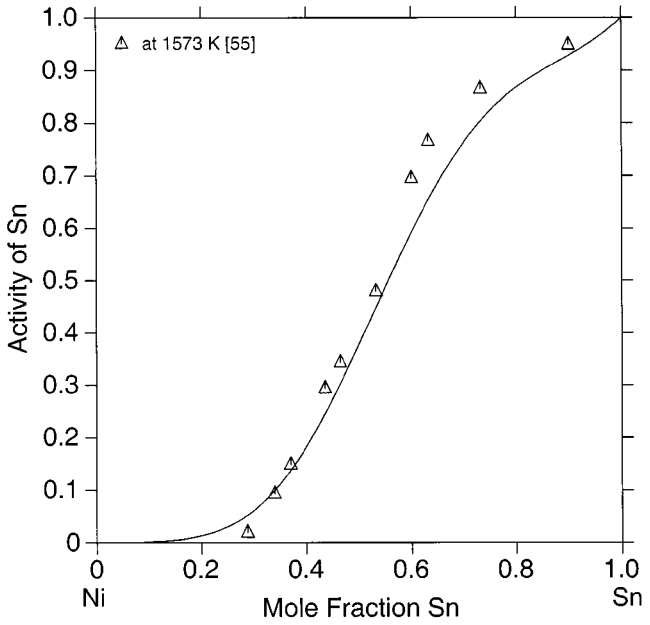

Fig. 7—The calculated activity of Sn in liquid Ni-Sn alloys at 1573 K is compared with the experimental data.[55] The reference states are fcc-Ni and liquid-Sn.

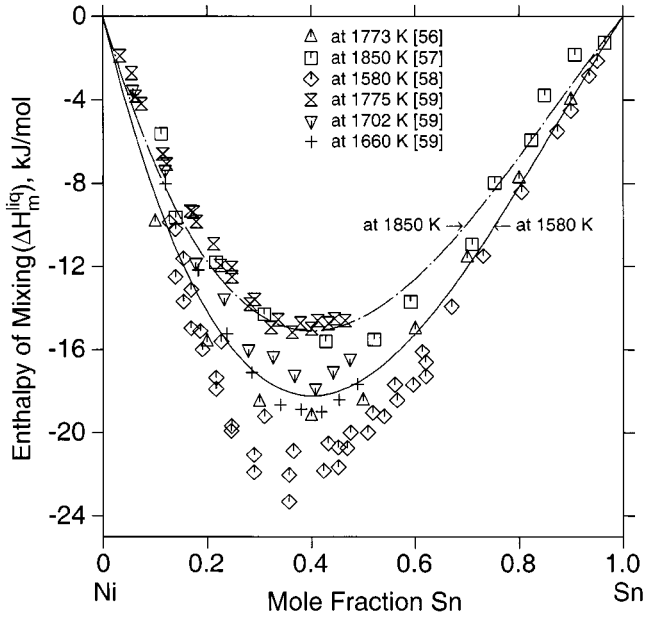

Fig. 8—The calculated enthalpies of mixing of liquid Ni-Sn alloys (ΔH_m^{liq}) at 1580 and 1850 K are compared with the experimental data.[56–59]

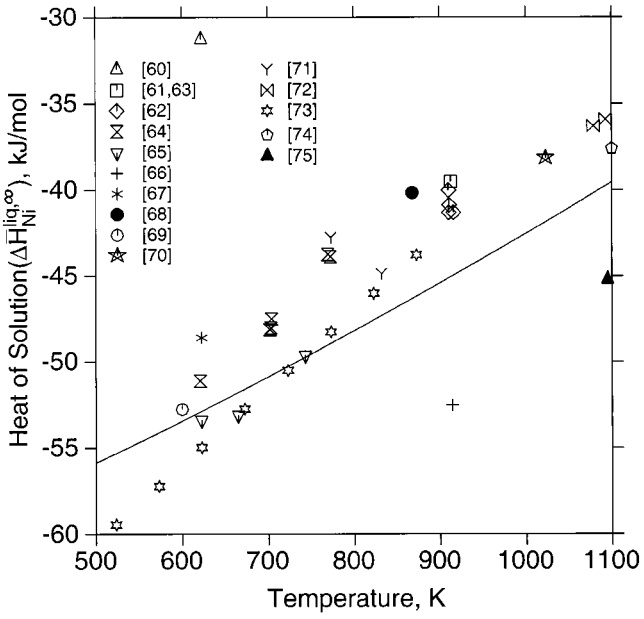

Fig. 9—The temperature dependence of the heat of solution of Ni at infinite dilution ($\Delta \overline{H}_{Ni}^{liq,\infty}$) in liquid Sn.[60–75] The solid line represents calculated values at 0.1 at. pct Ni. The reference states are fcc-Ni and liquid-Sn.

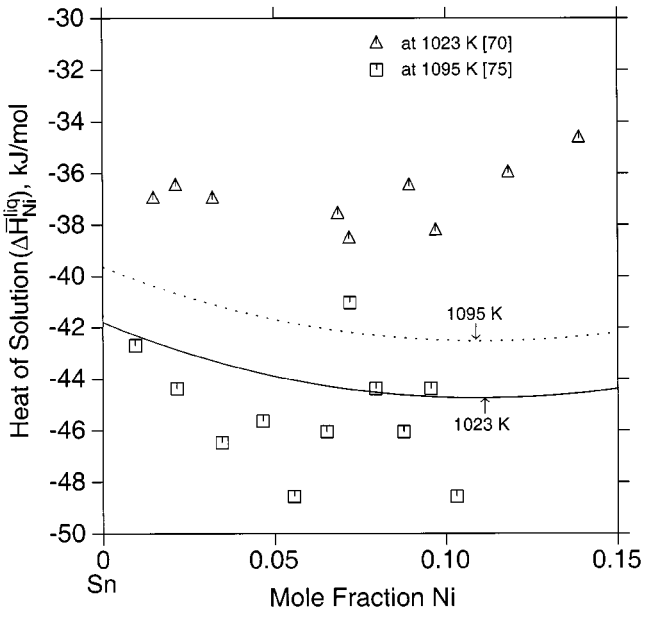

Fig. 10—The partial molar heats of solution of Ni ($\Delta \overline{H}_{Ni}^{liq}$) in the liquid Ni-Sn alloy are compared with the experimental values[70,75] at 1023 and 1095 K. The reference states are fcc-Ni and liquid-Sn.

and Vogelbein[77] and show only a reasonable agreement with the predicted values.[109]

Figure 11 shows the temperature dependence of the calculated order parameter ξ (equal to $Y_{Ni}^{III} - Y_{Ni}^{IV}$) of λ-Ni_3Sn_2. As expected, there is a deviation in the shape of the curves as the composition deviates from the ideal composition of 40 at. pct Sn. Also, the critical temperature for ordering decreases with increasing Sn content. However, the rate of decrease in the calculated critical temperature with composition is milder than the experimental value of Fjellvag and Kjekshus,[92] who reported a decrease in critical temperature by 90 K as the composition changes from 40 to 41 at. pct Sn.

Figure 12 shows the calculated Pb-Sn phase diagram using the thermodynamic parameters of Ngai and Chang.[4]

Figures 13 through 18 show the calculated isothermal sections of the Ni-Pb-Sn system at 598, 533, 513, 493, 473, and 398 K, respectively. In the absence of experimental data, the solid solubility of Pb in the Ni-Sn intermediate phases were neglected. The presence of a very narrow three-phase field of liquid + λ-Ni_3Sn_2 + (Pb) may be noted in Figure 13. It may also be noted that, in the temperature range from 473 to 598 K, the solubility of Ni in the liquid solder is negligible. This is in contrast to the Pd-Pb-Sn system, where

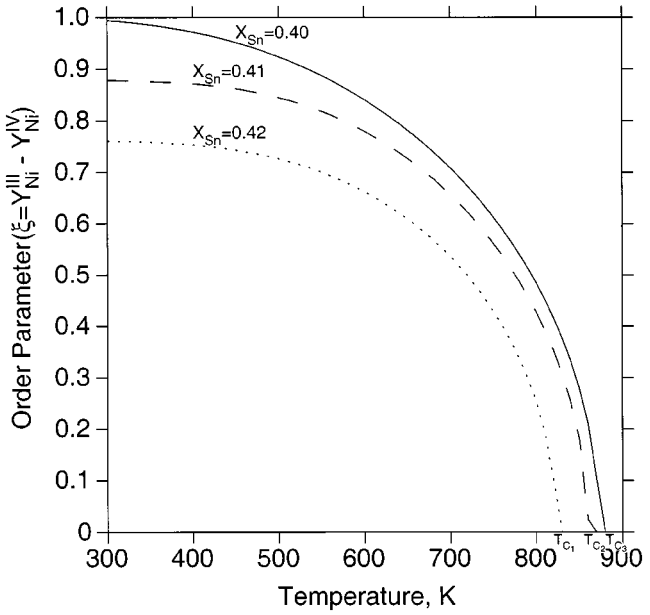

Fig. 11—The temperature dependence of the order parameter of λ-Ni_3Sn_2 as a function of its Sn content.

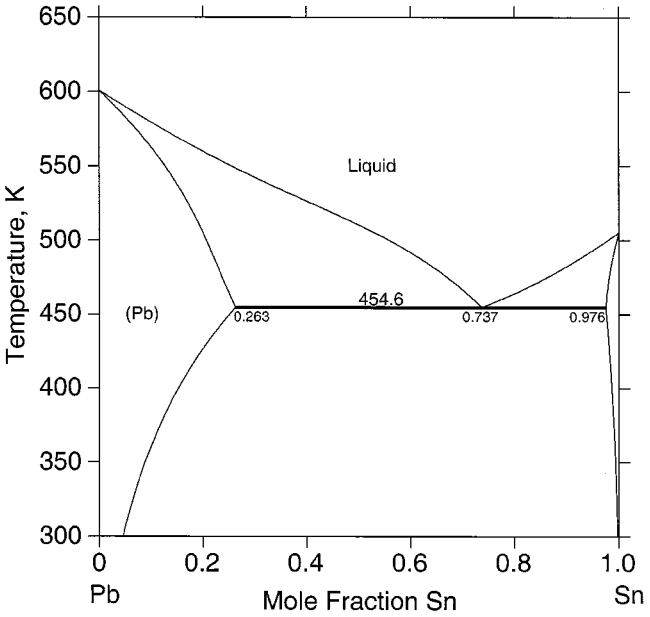

Fig. 12—The calculated Pb-Sn phase diagram.[4]

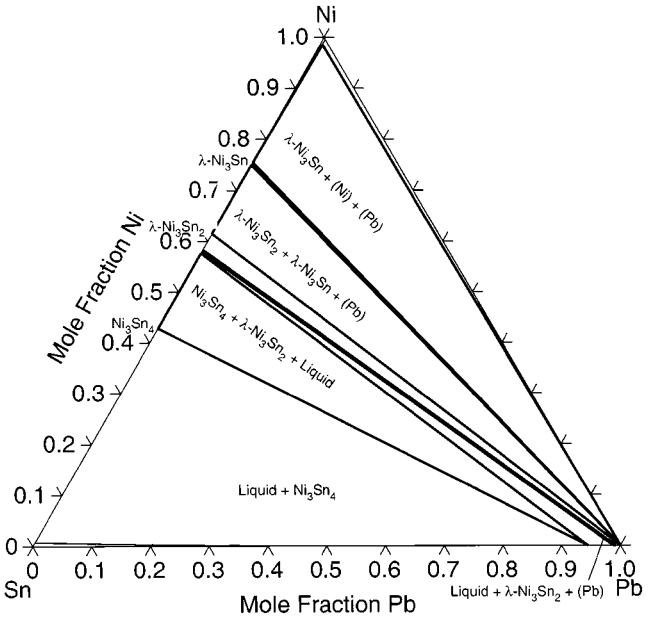

Fig. 13—The calculated isothermal section of the Ni-Pb-Sn system at 598 K.

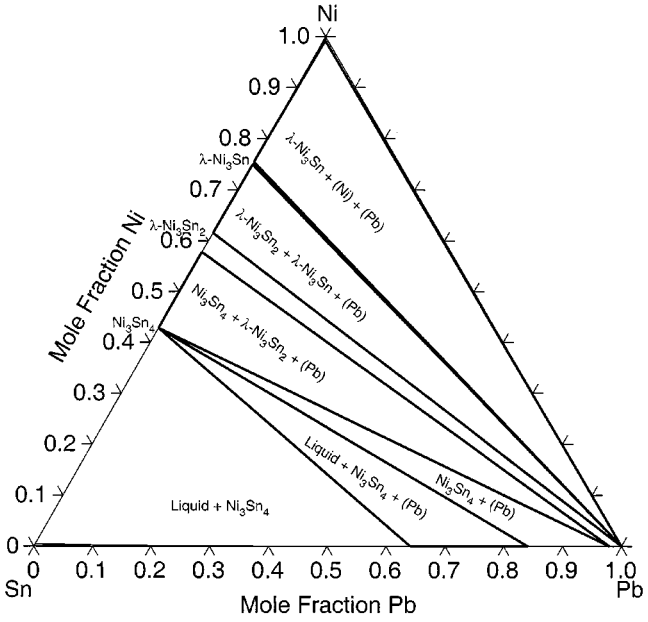

Fig. 14—The calculated isothermal section of the Ni-Pb-Sn system at 533 K.

a solubility up to several atomic percentages of Pd in liquid solder was predicted in the same temperature range.[94] In Figures 13 through 17, the two-phase field of liquid + Ni_3Sn_4 becomes smaller as the temperature decreases. In the solid state, the topology of the isothermal sections remains the same as that shown in Figure 18. Therefore, the isothermal section shown in Figure 18 can also be used at other temperatures, as long as all phases are solid. The aforementioned ternary-phase diagrams are of practical interest for understanding and interpreting the diffusion path or the interfacial microstructure that develops due to the reaction between Pb-Sn solders and Ni metallizations.

VI. CONCLUSIONS

Thermodynamic modeling of the Ni-Pb and Ni-Sn systems is presented. A set of self-consistent model parameters are optimized using a computer-aided approach. In most cases, the agreement between the calculated and experimental values is very good. The intermediate phases having a finite solid solubility are described by the compound-energy formalism. A two-sublattice model is used to describe the molar Gibbs energies of the η-Ni_3Sn_2, λ-Ni_3Sn_2, and Ni_3Sn_4 phases. A three-sublattice model is used to describe the molar Gibbs energy of the η-Ni_3Sn_2 phase, and a four-sublattice model is adopted for the λ-Ni_3Sn_2 phase. The

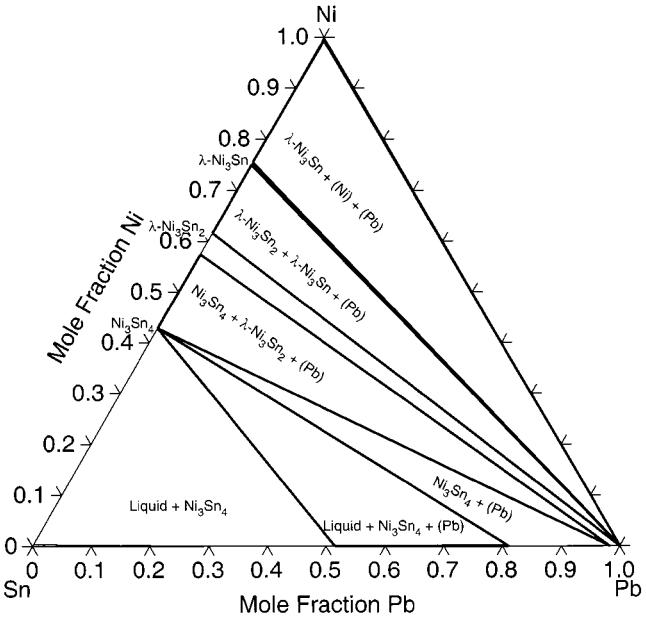

Fig. 15—The calculated isothermal section of the Ni-Pb-Sn system at 513 K.

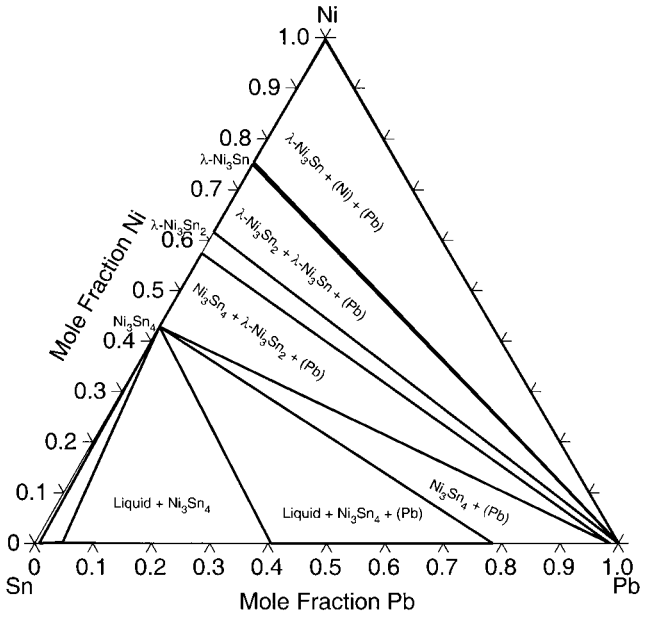

Fig. 16—The calculated isothermal section of the Ni-Pb-Sn system at 493 K.

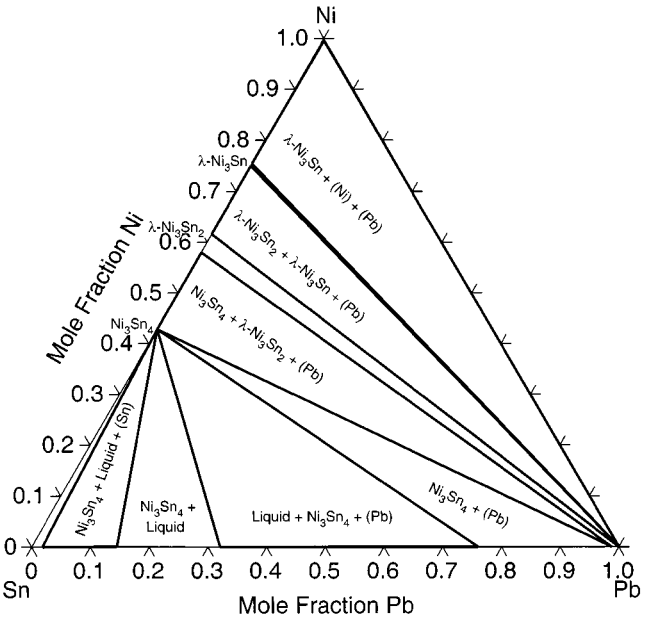

Fig. 17—The calculated isothermal section of the Ni-Pb-Sn system at 473 K.

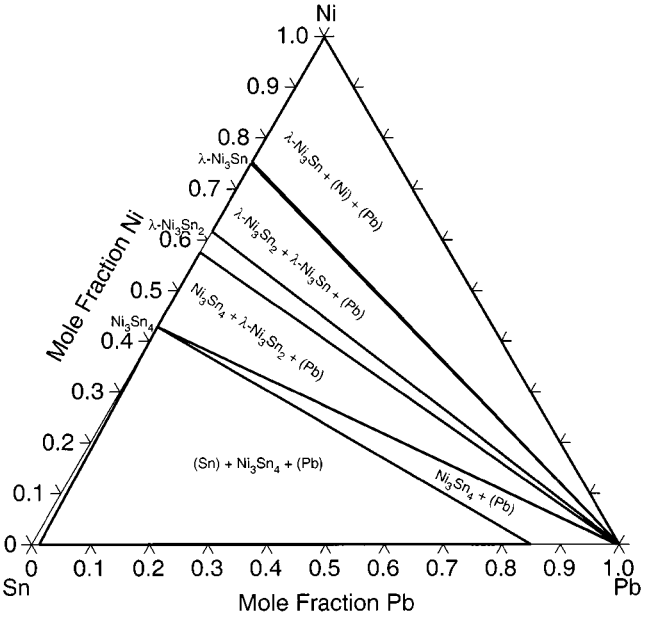

Fig. 18—The calculated isothermal section of the Ni-Pb-Sn system at 398 K.

η-Ni_3Sn_2 phase undergoes a second-order phase transition around 873 K, leading to ordering of Ni and vacancies. The aforementioned sublattice models for the Ni_3Sn_2 phase are consistent with this second-order phase transition. The ternary solid solubility of the intermediate phases and the existence of a ternary phase, if any, are presently unknown. Using the thermodynamic model parameters, several isothermal sections of the Ni-Pb-Sn system are calculated. The temperature range covered in the calculated isothermal sections is consistent with both the processing temperatures for wave and reflow soldering and the operating temperatures of the electronic devices. The calculated isothermal sections are of practical importance for understanding the diffusion path, interfacial reactions/microstructure, and metastability in diffusion couples of the Ni-Pb-Sn system, relevant to microelectronic packaging. Present thermodynamic modeling also lays the foundation for kinetic modeling of the interfacial phase(s) formed during reaction between the Ni and Pb-Sn solders in the liquid and solid states, and also for understanding the diffusion path (or the interfacial microstructure) between the Ni-and Sn-containing Pb-free solders.

ACKNOWLEDGMENTS

This work was supported by the National Science Foundation (Grant No. DMR-9523447 and DMR-9813919). All

Table III. A Comparison of Optimized (This Study), Measured,[56,70,76,77] and Predicted[109] Heat of Formation of Ni-Sn Intermediate Phases

Phase	Heat of Formation (kJ/mol)	Reference
λ-Ni_3Sn	−26.310*	77
	−19*	109
	−26.657*	this study
λ-Ni_3Sn_2	−31.280**	56
	−38.519*	76
	−31.790*	77
	−24*	109
	−30.322*	this study
η-Ni_3Sn_2	−38.644†	70
	−32.871†	this study
Ni_3Sn_4	−25.330*	77
	−25.409*	this study
	−33.704†	70
	−29.359†	this study

*Standard heat of formation ($\Delta H_f^{298.15}$) (reference states are fcc-Ni and bct-Sn).
**At 273 K (reference states are fcc-Ni and bct-Sn).
†At 1023 K (reference states are fcc-Ni and liquid-Sn).

thermodynamic optimizations and calculations were performed using PARROT and Thermo-Calc, respectively, developed by Drs. B. Sundman, B. Jansson, and J.-O. Andersson, Royal Institute of Technology (Stockholm).

APPENDIX

The following are thermodynamic parameters of the Ni-Pb-Sn system. The excess parameters for liquid, fcc, and bct phases of the Pb-Sn system are taken from Ngai and Chang.[4] The lattice stabilities of pure elements are taken from the SGTE database.[78] All parameters are in Joules per mole and T is in Kelvin.

Liquid phase:
Ni,Pb,Sn::1
$^\circ G_{Ni}^{liq} - H_{Ni}^{SER} = GNILIQ$
$^\circ G_{Pb}^{liq} - H_{Pb}^{SER} = GPBLIQ$
$^\circ G_{Sn}^{liq} - H_{Sn}^{SER} = GSNLIQ$
$L_{Ni,Pb}^{0,liq} = 20{,}506.2970 + 4.9289\ T$
$L_{Ni,Pb}^{1,liq} = 7353.4737 - 1.9517\ T$
$L_{Ni,Pb}^{2,liq} = 2966.2970 + 0.8579\ T$
$L_{Ni,Pb}^{3,liq} = -1792.3800 + 0.9434\ T$
$L_{Ni,Pb}^{4,liq} = -3781.4910$
$L_{Ni,Sn}^{0,liq} = -140{,}308.4825 + 386.8963\ T - 44.6662\ T \ln T$
$L_{Ni,Sn}^{1,liq} = -60{,}955.5766 + 155.5473\ T - 18.8184\ T \ln T$
$L_{Pb,Sn}^{0,liq} = 5125 + 1.4642\ T$
$L_{Pb,Sn}^{1,liq} = 293.82$

Fcc phase:
Ni,Pb,Sn::1
$^\circ G_{Ni}^{fcc} - H_{Ni}^{SER} = GHSERNI$
$\beta_{Ni}^{fcc} = 0.604$
$T_{CNi}^{fcc} = 633$
$^\circ G_{Pb}^{fcc} - H_{Pb}^{SER} = GHSERPB$
$^\circ G_{Sn}^{fcc} - H_{Sn}^{SER} = GFCCSN$
$L_{Ni,Pb}^{0,fcc} = 15{,}235.3889 + 24.1891\ T$
$L_{Ni,Pb}^{1,fcc} = -6641.6489 + 4.4906\ T$
$L_{Ni,Sn}^{0,fcc} = -60{,}397.1938 + 5.9676\ T$
$L_{Ni,Sn}^{1,fcc} = -25{,}786.9564 + 4.9201\ T$
$\beta_{Ni,Sn}^{0,fcc} = -6.8002$
$\beta_{Ni,Sn}^{1,fcc} = 4.3689$
$T_{C;Ni,Sn}^{0,fcc} = -13{,}907$
$T_{C;Ni,Sn}^{1,fcc} = 12{,}998$
$L_{Pb,Sn}^{0,fcc} = 5132.4154 + 1.5631\ T$

Bct phase:
Ni,Pb,Sn::1
$^\circ G_{Ni}^{bct} - {}^\circ G_{Ni}^{fcc} = 10{,}023 - 4.556\ T$
$^\circ G_{Pb}^{bct} - {}^\circ G_{Pb}^{fcc} = 489 + 3.52\ T$
$^\circ G_{Sn}^{bct} - H_{Sn}^{SER} = GHSERSN$
$L_{Ni,Sn}^{0,bct} = -21{,}500$
$L_{Pb,Sn}^{0,bct} = 17{,}117.7858 - 11.8066\ T$

η-Ni_3Sn phase (high-temperature Ni_3Sn):
Ni,Sn:Sn,Ni::0.75:0.25
$^\circ G_{Ni:Ni}^{\eta\text{-}Ni_3Sn} - H_{Ni}^{SER} = GBCCNI$
$^\circ G_{Ni:Sn}^{\eta\text{-}Ni_3Sn} - 0.75\ {}^\circ G_{Ni}^{fcc} - 0.25\ {}^\circ G_{Sn}^{bct} = GNI3SNHT$
$^\circ G_{Sn:Ni}^{\eta\text{-}Ni_3Sn} - 0.25\ {}^\circ G_{Ni}^{fcc} - 0.75\ {}^\circ G_{Sn}^{bct} = GBCCNI + GBCCSN - GNI3SNHT$
$^\circ G_{Sn:Sn}^{\eta\text{-}Ni_3Sn} - H_{Sn}^{SER} = GBCCSN$
$L_{Ni:Ni,Sn}^{0,\eta\text{-}Ni_3Sn} = 18{,}404.5756 - 11.8855\ T$
$L_{Sn:Ni,Sn}^{0,\eta\text{-}Ni_3Sn} = 18{,}404.5756 - 11.8855\ T$
$L_{Ni,Sn:Ni}^{0,\eta\text{-}Ni_3Sn} = -20{,}649.7462 + 4.2325\ T$
$L_{Ni,Sn:Sn}^{0,\eta\text{-}Ni_3Sn} = -20{,}649.7462 + 4.2325\ T$

λ-Ni_3Sn phase (low-temperature Ni_3Sn):
Ni,Sn:Sn,Ni::0.75:0.25
$^\circ G_{Ni:Ni}^{\lambda\text{-}Ni_3Sn} - H_{Ni}^{SER} = GHCPNI$
$^\circ G_{Ni:Sn}^{\lambda\text{-}Ni_3Sn} - 0.75\ {}^\circ G_{Ni}^{fcc} - 0.25\ {}^\circ G_{Sn}^{bct} = GNI3SNLT$
$^\circ G_{Sn:Ni}^{\lambda\text{-}Ni_3Sn} - 0.25\ {}^\circ G_{Ni}^{fcc} - 0.75\ {}^\circ G_{Sn}^{bct} = GHCPNI + GHCPSN - GNI3SNLT$
$^\circ G_{Sn:Sn}^{\lambda\text{-}Ni_3Sn} - H_{Sn}^{SER} = GHCPSN$
$L_{Ni:Ni,Sn}^{0,\lambda\text{-}Ni_3Sn} = -1510.5943 + 7.3684\ T$
$L_{Sn:Ni,Sn}^{0,\lambda\text{-}Ni_3Sn} = -1510.5943 + 7.3684\ T$
$L_{Ni,Sn:Ni}^{0,\lambda\text{-}Ni_3Sn} = -20{,}578.9458 + 5.2632\ T$
$L_{Ni,Sn:Sn}^{0,\lambda\text{-}Ni_3Sn} = -20{,}578.9458 + 5.2632\ T$

η-Ni_3Sn_2 phase (high-temperature Ni_3Sn_2):
Ni:Sn:Ni,Va::1:1:1
$^\circ G_{Ni:Sn:Ni}^{\eta\text{-}Ni_3Sn_2} - 2{}^\circ G_{Ni}^{fcc} - {}^\circ G_{Sn}^{bct} = GNI2SN$
$^\circ G_{Ni:Sn:Va}^{\eta\text{-}Ni_3Sn_2} - {}^\circ G_{Ni}^{fcc} - {}^\circ G_{Sn}^{bct} = GNISN$
$L_{Ni:Sn:Ni,Va}^{0,\eta\text{-}Ni_3Sn_2} = L0NI3SN2$
$L_{Ni:Sn:Ni,Va}^{1,\eta\text{-}Ni_3Sn_2} = L1NI3SN2$

λ-Ni_3Sn_2 phase (low-temperature Ni_3Sn_2):
Ni:Sn:Ni,Va:Ni,Va::1:1:0.5:0.5
$^\circ G_{Ni:Sn:Ni:Ni}^{\lambda\text{-}Ni_3Sn_2} - 2{}^\circ G_{Ni}^{fcc} - {}^\circ G_{Sn}^{bct} = GNI2SN$
$^\circ G_{Ni:Sn:Ni:Va}^{\lambda\text{-}Ni_3Sn_2} - 1.5{}^\circ G_{Ni}^{fcc} - {}^\circ G_{Sn}^{bct} = WNI3SN2 + 0.5\ GNI2SN + 0.5\ GNISN + 0.25\ L0NI3SN2$
$^\circ G_{Ni:Sn:Va:Ni}^{\lambda\text{-}Ni_3Sn_2} - 1.5{}^\circ G_{Ni}^{fcc} - {}^\circ G_{Sn}^{bct} = WNI3SN2 + 0.5\ GNI2SN + 0.5\ GNISN + 0.25\ L0NI3SN2$
$^\circ G_{Ni:Sn:Va:Va}^{\lambda\text{-}Ni_3Sn_2} - {}^\circ G_{Ni}^{fcc} - {}^\circ G_{Sn}^{bct} = GNISN$
$L_{Ni:Sn:Ni,Va:Ni}^{0,\lambda\text{-}Ni_3Sn_2} = -WNI3SN2 + 0.25\ L0NI3SN2 + 0.375\ L1NI3SN2$
$L_{Ni:Sn:Ni,Va:Va}^{0,\lambda\text{-}Ni_3Sn_2} = -WNI3SN2 + 0.25\ L0NI3SN2 - 0.375\ L1NI3SN2$
$L_{Ni:Sn:Ni:Ni,Va}^{0,\lambda\text{-}Ni_3Sn_2} = -WNI3SN2 + 0.25\ L0NI3SN2 + 0.375\ L1NI3SN2$
$L_{Ni:Sn:Va:Ni,Va}^{0,\lambda\text{-}Ni_3Sn_2} = -WNI3SN2 + 0.25\ L0NI3SN2 - 0.375\ L1NI3SN2$
$L_{Ni:Sn:Ni,Va:Ni}^{1,\lambda\text{-}Ni_3Sn_2} = 0.125\ L1NI3SN2$
$L_{Ni:Sn:Ni,Va:Va}^{1,\lambda\text{-}Ni_3Sn_2} = 0.125\ L1NI3SN2$

$L^{1,\lambda\text{-}Ni_3Sn_2}_{Ni:Sn:Ni:Ni,Va}$ = 0.125 L1NI3SN2
$L^{1,\lambda\text{-}Ni_3Sn_2}_{Ni:Sn:Va:Ni,Va}$ = 0.125 L1NI3SN2

Ni_3Sn_4 phase:
Ni:Sn,Ni::0.4286:0.5714
$^\circ G^{Ni_3Sn_4}_{Ni:Ni} - {}^\circ G^{fcc}_{Ni} = 5000$
$^\circ G^{Ni_3Sn_4}_{Ni:Sn} - 0.4286\ ^\circ G^{fcc}_{Ni} - 0.5714\ ^\circ G^{bct}_{Sn} = -25{,}180.3905 + 2.1289\ T$
$L^{0,Ni_3Sn_4}_{Ni:Ni,Sn} = -11{,}991.4575$
$L^{1,Ni_3Sn_4}_{Ni:Ni,Sn} = 9991.4395$

Symbols:
GNILIQ = 11,235.527 + 108.457 T − 22.096 T ln T − 0.0048407 T^2 −3.82318 × 10^{-21} T^7; for 298.15 ≤ T ≤ 1728
GNILIQ = −9549.775 + 268.598 T − 43.1 T ln T; for 1728 ≤ T ≤ 3000
GHSERNI = −5179.159 + 117.854 T − 22.096 T ln T − 0.0048407 T^2; for 298.15 ≤ T ≤ 1728
GHSERNI = −27,840.655 + 279.135 T − 43.1 T ln T + 1.12754 × 10^{31} T^{-9}; for 1728 ≤ T ≤ 3000
GPBLIQ = 4672.157 − 7.750257 T − 6.0144 × 10^{-19} T^7 + GHSERPB; for 298.15 ≤ T ≤ 600.65
GPBLIQ = 4853.112 − 8.066587 T − 8.05644 × 10^{25} T^{-9} + GHSERPB; for 600.65 ≤ T ≤ 5000
GSNLIQ = 6970.705 − 13.813302 T + 1.24912 × 10^{25} T^{-9} + GHSERSN; for 505.06 ≤ T ≤ 3000
GHSERPB = −7650.085 + 101.715188 T − 24.5242231 T ln T −0.00365895 T^2 − 2.4395 × 10^{-7} T^3; for 298.15 ≤ T ≤ 600.65
GHSERPB = −10,531.115 + 154.258155 T − 32.4913959 T ln T + 0.00154613 T^2 +8.05644 × 10^{25} T^{-9}; for 600.65 ≤ T ≤ 1200
GHSERPB = 4157.596 + 53.154045 T − 18.9640637 T ln T − 0.002882943 T^2 +9.8144 × 10^{-8} T^3 − 2,696,755 T^{-1} + 8.05644 × 10^{25} T^{-9}; for 1200 ≤ T ≤ 5000
GHSERSN = −7958.517 + 122.750027 T − 25.858 T ln T +5.1185 × 10^{-4} T^2 − 3.192767 × 10^{-6} T^3 + 18,440 T^{-1}; for 100 ≤ T ≤ 250
GHSERSN = −5855.135 + 65.427891 T − 15.961 T ln T − 0.0188702 T^2 + 3.121167 × 10^{-6} T^3 −61,960 T^{-1}; for 250 ≤ T ≤ 505.08
GHSERSN = 2524.724 + 3.989845 T − 8.2590486 T ln T − 0.016814429 T^2 +2.623131 × 10^{-6} T^3 − 1,081,244 T^{-1} − 1.2307 × 10^{25} T^{-9}; for 505.08 ≤ T ≤ 800
GHSERSN = −8256.959 + 138.981456 T − 28.4512 T ln T − 1.2307 × 10^{25} T^{-9}; for 800 ≤ T ≤ 3000
GBCCNI = 8715.084 − 3.556 T + GHSERNI
GHCPNI = 1046 + 1.255 T + GHSERNI
GHCPSN = 3900 − 4.4 T + GHSERSN
GBCCSN = 4400 − 6 T + GHSERSN
GFCCSN = 4150 − 5.2 T + GHSERSN
GNI3SNHT = −26,538.1585 + 4.0981 T
GNI3SNLT = −26,657.4693 + 4.1849 T
GNI2SN = −84,327 + 13.3696 T
GNISN = −44,207 + 3.6562 T
WNI3SN2 = −3630
L0NI3SN2 = −44,219.3584 + 12.1951 T
L1NI3SN2 = 20,000

REFERENCES

1. D.C. Abbott, R.M. Brook, N. McLelland, and J.S. Wiley: *IEEE Trans. Compon. Hybrids Manuf. Technol.*, 1991, vol. 14, pp. 567-72.
2. S.K. Kang, R.S. Rai, and S. Purusothaman: *J. Electronic Mater.*, 1996, vol. 25, pp. 1113-20.
3. I. Karakaya and W.T. Thompson: *Bull. Alloy Phase Diagrams*, 1988, vol. 9, pp. 144-52.
4. T.L. Ngai and Y.A. Chang: *CALPHAD*, 1983, vol. 5, pp. 267-76.
5. P. Nash: *Bull. Alloy Phase Diagrams*, 1987, vol. 8, pp. 264-68.
6. P. Nash and A. Nash: *Bull. ALloy Phase Diagrams*, 1985, vol. 6, pp. 350-59.
7. C. R. Cavanaugh and J.F. Elliot: *Trans. TMS-AIME*, 1964, vol. 230, pp. 633-38.
8. T. Alden, D.A. Stevenson, and J. Wulff: *Trans. TMS-AIME*, 1958, vol. 212, pp. 15-17.
9. M.A. Portevin: *Rev. Metall.*, 1907, vol. 4, pp. 814-18.
10. G. Voss: *Z. Anorg. Chem.*, 1908, vol. 57, pp. 45-48.
11. E. Pelzel: *Metallurgy*, 1955, vol. 9, pp. 692-94.
12. B. Fleischer and J.F. Elliot: in *The Physical Chemistry of Metallic Solutions and Intermetallic Compounds*, [Proc. Symp. No. 9,] National Physical Laboratory, Teddington, United Kingdom, 1959, vol. 1, p. 12.
13. K.O. Miller and J.F. Elliot: *Trans. TMS-AIME*, 1960, vol. 218, pp. 900-10.
14. T.R.A. Davey: *Physical Chemistry of Process Metallurgy*, TMS-AIME Conf., TMS-AIM, Warrendale, PA, 1961, vol. 7, pp. 581-600.
15. A. Taskinen: *Scand. J. Metall.*, 1981, vol. 10, pp. 185-88.
16. G. Tammann and G. Bandel: *Z. Metallkd.*, 1933, vol. 25, p. 156.
17. T. Pomianek: *Z. Metallkd.*, 1986, vol. 77, pp. 388-92.
18. G. Tammann and W. Oelsen: *Z. Anorg. Chem.*, 1930, vol. 186, pp. 266-67.
19. R. Nozato, T. Morigaki, and H. Tsubakino: *Trans. Jpn. Inst. Met.*, 1983, vol. 24, pp. 18-23.
20. M. Hansen and K. Anderko: *Constitution of Binary Alloys*, McGraw-Hill Book Company, Inc., New York, NY, 1958.
21. W. Hoffmann: *Lead and Lead Alloys*, Springer-Verlag, Berlin, 1970, p. 69.
22. R. Ricci-Bitti, J. Dixmier, and A. Guinier: *Compt. Rend. B*, 1968, vol. 266, pp. 565-67.
23. B.C. Giessen: in *Rapidly Quenched Metals*, N.J. Grant and B.C. Giessen, eds., MIT, Cambridge, MA, 1976, pp. 119-34.
24. J.F. Freedman and A.S. Nowick: *Acta Metall.*, 1958, vol. 6, pp. 176-83.
25. B. Predel and H. Sandig: *Z. Metallkd.*, 1969, vol. 60, pp. 208-14.
26. C.T. Heycock and F.H. Neville: *J. Chem. Soc.*, 1890, vol. 57, p. 378.
27. H. Gautier: *Bull. Soc. Encour. Ind. Nat.*, 1896, vol. 1, p. 1313.
28. M.L. Guillet: *Rev. Met.*, 1907, vol. 4, pp. 535-51.
29. M.L. Guillet: *Compt. Rend. Acad. Sci.*, 1907, vol. 144, pp. 752-53.
30. G. Voss: *Z. Anorg. Chem.*, 1908, vol. 57, pp. 35-45.
31. D. Hanson, E.S. Sandford, and H. Stevens: *J. Inst. Met.*, 1934, vol. 55, pp. 117-19.
32. E.R. Jette and E. Fetz: *Metallwirt. Wiss. Technol.*, 1935 vol. 14, pp. 165-68.
33. W. Mikulus, L. Thomassen, and C. Upthegrove: *Trans. AIME, Inst. Met. Div.*, 1937, vol. 124, pp. 111-37.
34. T. Heumann: *Z. Metallkd.*, 1943, vol. 35, pp. 206-11.
35. M.G. Charpy: *Bull. Soc. Encour. Ind. Nat.*, 1897, vol. 2, pp. 384-419.
36. E. Vigouroux: *Comp. Rend. Acad. Sci.*, 1907, vol. 144, pp. 639-41.
37. E. Vigouroux: *Comp. Rend. Acad. Sci.*, 1907, vol. 144, pp. 712-14.
38. E. Vigouroux: *Comp. Rend. Acad. Sci.*, 1907, vol. 144, pp. 1351-53.
39. E. Vigouroux: *Comp. Rend. Acad. Sci.*, 1907, vol. 145, pp. 246-48.
40. E. Vigouroux: *Comp. Rend. Acad. Sci.*, 1907, vol. 145, pp. 429-31.
41. I. Oftedal: *Z. Phys. Chem.*, 1928, vol. 132, pp. 208-16.
42. E. Fetz and E.R. Jette: *J. Chem. Phys.*, 1936, vol. 4, p. 537.
43. E. Fetz and E.R. Jette: *Trans. AIME*, 1937, vol. 124, pp. 133-36.
44. H. Nowotny and K. Schubert: *Naturwissenschaften*, 1944, vol. 32, p. 76.
45. H. Nowotny and K. Schubert: *Z. Metallkd.*, 1946, vol. 37, pp. 23-31.
46. F. Lihl and H. Kirnbauer: *Monatsh. Chem.*, 1955, vol. 86, pp. 745-51.
47. F. Lihl and H. Kirnbauer: *Z. Metallkd.*, 1955, vol. 46, pp. 438-39.
48. L.A. Panteleimonov, A.Y. Khanna, I.G. Sokolova, and A.K. Bagdasaryan: *Vestn. Mosk. Univ. Ser. II: Khim.*, 1964, vol. 19, pp. 45-50.
49. O. Nial: *Svesk Kemisk Tidskrift*, 1947, vols. 59–60, pp. 172-83.
50. M.K. Bhargava and K. Schubert: *J. Less-Common Met.*, 1973, vol. 33, pp. 181-89.
51. W. Michel: *Ann. Phys.*, 1963, vol. 11, pp. 321-53.
52. P. Rahlfs: *Metallwirtschaft*, 1937, vol. 16, pp. 343-45.
53. C. Djega-Mariadassou: *Ann. Chim. (Paris)*, 1970, vol. 5, pp. 497-504.
54. V.N. Eremenko, G.M. Lukashenko, and V.L. Pritula: *Russ. J. Phys. Chem.*, 1971, vol. 45, pp. 1131-32.
55. V.N. Eremenko, G.M. Lukashenko, and V.L. Pritula: *Proc. 4th Int.*

Conf. Vacuum Metallurgy, Iron and Steel Institute of Japan, Tokyo, 1973, pp. 44-46.
56. F. Koerber and W. Oelson: *Mitt. Kaiser Wilh. Inst. Eisenforsch.*, 1937, vol. 19, pp. 209-19.
57. Y.O. Esin, V.M. Baev, and S.N. Morozov: *Fiz. Svoistva Met. Splavov*, 1976, vol. 1, pp. 66-72.
58. M.J. Pool, I. Arpshofen, B. Predel, and E. Schultheiβ: *Z. Metallkd.*, 1979, vol. 70, pp. 656-59.
59. R. Luck, J. Tomiska, and B. Predel: *Z. Metallkd.*, 1988, vol. 79, pp. 345-49.
60. J.S.L. Leach and M.B. Bever: *Trans. AIME*, 1959, vol. 43, p. 248.
61. R.A. Oriani and W.K. Murphy: *Acta Metall.*, 1960, vol. 8, pp. 23-25.
62. G.F. Day and R. Hultgern: *J. Phys. Chem.*, 1962, vol. 66, pp. 1532-34.
63. R. Oriani and W.K. Murphy: *Acta Metall.*, 1962, vol. 10, pp. 879-85.
64. R.C. King and O.J. Kleppa: *Acta Metall.*, 1964, vol. 12, pp. 87-97.
65. J. Hertz: *C.R. Acad. Sci., Paris, Ser. C*, 1966, vol. 232, pp. 1652-54.
66. R.A. Walker and J.B. Darby: *Acta Metall.*, 1970, vol. 18, pp. 1261-66.
67. A.K. Jena and T.R. Ramachandran: *Scripta Metall.*, 1971, vol. 5, pp. 639-42.
68. B. Predel and H. Ruge: *Mater. Sci. Eng.*, 1972, vol. 9, pp. 141-51.
69. R. Boom: *Scripta Metall.*, 1974, vol. 8, pp. 1277-82.
70. H.-D. Dannohl and H.L. Lukas: *Z. Metallkd.*, 1974, vol. 65, pp. 642-49.
71. S. Martosudirjo and J.N. Pratt: *Thermochimica Acta*, 1976, vol. 17, pp. 183-94.
72. W. Vogelbein: *Ph.D. Thesis*, University of Stuttgart, Stuttgart, Germany, 1976.
73. J.C. Gachon, M. Notin, C. Cunat, J. Hertz, J.C. Parlebas, G. Moraitis, B. Stupfel, and F. Gautier: *Acta Metall.*, 1980, vol. 28, pp. 489-97.
74. W. Vogelbein, B. Predel, and Y.A. Chang: *Z. Metallkd.*, 1982, vol. 73, pp. 530-33.
75. J. Schott and F. Sommer: *J. Less-Common Met.*, 1986, vol. 119, pp. 307-17.
76. B. Predel and H. Ruge: *Thermochimica Acta*, 1972, vol. 3, pp. 411-19.
77. B. Predel and W. Vogelbein: *Thermochimica Acta*, 1979, vol. 30, pp. 201-05.
78. A. Dinsdale: NPL Report DMA (A) 195, National Physical Laboratory, Teddington, United Kingdom, 1989.
79. O. Redlich and A. Kister: *Ind. Eng. Chem.*, 1948, vol. 40, pp. 345-48.
80. M. Hillert and M. Jarl: *CALPHAD*, 1978, vol. 2, pp. 227-38.
81. D.H. Martin: *Magnetism in Solids*, MIT Press, Cambridge, MA, 1967, p. 10.
82. C. Manders: *Ann. Phys.*, 1936, vol. 5, pp. 167-231
83. V. Marian: *Ann. Phys.*, 1937, vol. 7, pp. 459-527.
84. K. Schubert, W. Burkhardt, P. Esslinger, E. Gunzel, H.G. Meissner, W. Schutt, J. Wegst, and M. Wilkens: *Naturwissenschaften*, 1956, vol. 43, pp. 248-49.
85. S.K. Shadangi, M. Singh, S.C. Panda, and S. Bhan: *Ind. J. Technol.*, 1986, vol. 24, pp. 105-07.
86. O.T. Woo, J. Rezek, and M. Schlesinger: *Mater. Sci. Eng.*, 1975, vol. 18, pp. 163-65.
87. W.B. Pearson and L.T. Thomson: *Can. J. Phys.* 1957, vol. 35, pp. 349-57.
88. J. Bandyopadhyay and K.P. Gupta: *Metall. Trans.*, 1970, vol. 1, pp. 327-29.
89. A. Schneider and K.H. Imhagen: *Naturwissenschaften*, 1957, vol. 44, p. 324.
90. P. Brand: *Wiss. Z. Martin Luther Univ. Halle Mitt.*, 1967, vol. 16, pp. 551-59.
91. P. Brand: *Z. Anorg. Chem.*, 1968, vol. 358, pp. 170-77.
92. H. Fjellvag and A. Kjekshus: *Acta Chem. Scand. A*, 1986, vol. 40A, pp. 23-30.
93. M. Ellner: *J. Less-Common Met.*, 1976, vol. 48, pp. 21-52.
94. G. Ghosh: *Metall. Mater. Trans. A*, 1997, vol. 30A, pp. 4-18.
95. G. Ghosh: *Met. Mater. Trans. A*, 1999, vol. 30A, pp. 5-18.
96. M. Asanuma: *J. Phys. Soc. Jpn.*, 1962, vol. 17, pp. 300-06.
97. K.C. Jain, M. Ellner, and K. Schubert: *Z. Metallkd.*, 1972, vol. 63, pp. 258-60.
98. J. Lacaze and B. Sundman: *Metall. Trans. A*, 1991, vol. 22A, pp. 2211-23.
99. M.E. Seiersten: in *Thermochemical Database for Light Metal Alloys*, Ed. I. Ansara (European Cooperation in the Field of Scientific and Technical Research, European Commission, Brussels, 1994), pp. 24-28.
100. M. Kowalski and P.J. Spencer: *J. Phase Equilibria*, 1993, vol. 14, pp. 432-38.
101. H. Nowotny and K. Schubert: *Naturwissenschaften*, 1944, vol. 32, p. 76.
102. H. Nowotny and K. Schubert: *Z. Metallkd.*, 1946, vol. 37, pp. 23-31.
103. W. Jeitschko and B. Jaberg: *Acta Crystallogr.*, 1982, vol. B38, pp. 598-600.
104. S. Furuseth and H. Fjellvag: *Acta Chem. Scand. A*, 1986, vol. 40A, pp. 695-700.
105. B. Jansson: *Trita-Mac-0234*, Royal Institute of Technology, Stockholm, 1984.
106. B. Sundman, B. Jansson, and J.O. Andersson: *CALPHAD*, 1985, vol. 9, pp. 153-90.
107. A. Bolcavage and U.R. Kattner: *J. Phase Equilibria*, 1996, vol. 17, pp. 92-100.
108. R.D. Agrawal, V.N.S. Mathur, and M.L. Kapoor: *Trans. Jpn. Inst. Met.*, 1980, vol. 21, pp. 1-8.
109. F.R. de Boer, R. Boom, W.C.M. Mattens, A.R. Miedema, and A.K. Niessen: *Cohesion in Metals, Transition Metals Alloys*, North-Holland, Amsterdam, 1988.